Electronic Supplementary Information

CPL on/off control of an assembled system by water soluble macrocyclic chiral sources with planar chirality

Shixin Fa, Takuya Tomita, Keisuke Wada, Kazuma Yasuhara, Shunsuke Ohtani, Kenichi Kato, Masayuki Gon, Kazuo Tanaka, Takahiro Kakuta, Tada-aki Yamagishi and Tomoki Ogoshi*

Table of Contents

General

All commercially available reagents and solvents were used as received. ^{1}H NMR, ^{13}C NMR and 2D COSY spectra were recorded on JEOL JNM-ECS400, JNM-ECZ500R and JNM-ECA600P spectrometers at room temperature. UV-vis absorption spectra, circular dichroism (CD) spectra and fluorescence spectra were recorded on a JASCO V-750 spectrophotometer, a JASCO J-1500 CD spectrometer and a Hitachi F-2500 fluorescence spectrophotometer, respectively. The absolute fluorescence quantum yield was measured by using an absolute PL quantum yield spectrometer Hamamatsu Quantamus-QY C11347. Circularly polarized luminescent (CPL) properties were measured on a JASCO J-810 spectrometer. 1 cm quartz cuvets were used. The fluorescence lifetime was performed on a Horiba FluoroCube spectrofluorometer system, and excitation was carried out using a UV diode laser (NanoLED 369 nm). The optical rotations of *R*-**1** and *S*-**1** were recorded on a Rudolph Research AUTOPOL IV Automatic Polarimete with the concentration of 0.1 M in methanol. High-resolution ESI-MS was recorded on Thermo Fisher Scientific Exactive Plus mass spectrometer equipped with UltiMate 3000 HPLC. Morphology of assemblies of **APy** was studied on a JEOL TEM-3100FEF microscope.

Syntheses

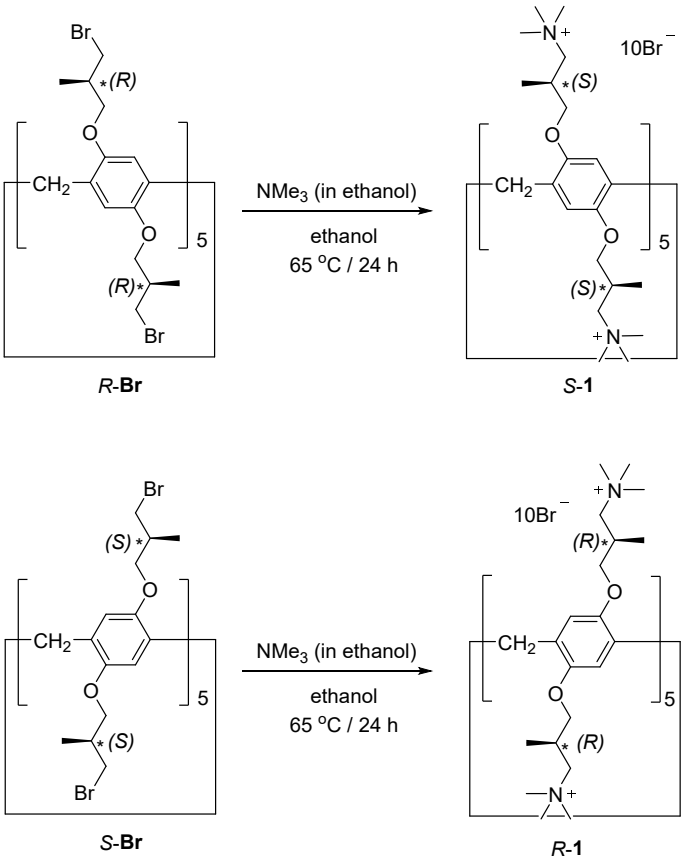

Scheme S1. Synthesis of *S*-**1** and *R*-**1**. Assignment of the stereo-centers is changed from (*S*)-

to (*R*)- and (*R*)- to (*S*)- by replacing the bromine atoms with trimethyl amine according to the Cahn-Ingold-Prelog priority rules.

Syntheses of per-alkylamino-substituted pillar[5]arene *R*-**Br**/*S*-**Br** and *S*-**Br**-unit were followed our reported procedure.[S1]

***S*-1.** To the solution of *R*-**Br** (100 mg, 0.05 mmol) in ethanol (5 mL) in a 50 mL round-bottom flask equipped with a condenser, trimethyl amine in ethanol (25%, 5 mL) was added slowly. The reaction mixture was heated to 65 °C and stirred for 24 hours. The solvent was evaporated. To the residual, DI water (10 mL) was added. The solution was washed thoroughly with chloroform (20 mL × 2). The solvent of the aqueous phase was evaporated, and the residual was dried in vacuum. The product was obtained as white solid (127 mg, yield: 98%). $[\alpha]^{23}_{D}$ = +26.2°. ^{1}H NMR (D_2O, 500 MHz, ppm): δ 6.72 (br, 10H), 4.11-3.60 (m, 30H), 3.50-3.23 (m, 20H) 3.03 (s, 90H), 2.43 (br, 10H), 1.11 (br, 30H). ^{13}C NMR (D_2O, 125 MHz, ppm): δ 149.8, 129.4, 116.0, 72.4, 69.9, 59.6, 53.5, 28.7, 17.8. ESI-HRMS. Calcd for $C_{105}H_{190}Br_{10}N_{10}O_{10}$ $[M-2Br]^{2+}$: 1195.4020, found 1195.4067; $[M-3Br]^{3+}$: 769.9624, found 769.9574.

***R*-1.** This compound was prepared by the same procedure as *S*-**1** from *S*-**Br** (100 mg, 0.05 mmol) and obtained as white solid (66 mg, yield: 50%). $[\alpha]^{23}_{D}$ = -15.3°. ^{1}H NMR (D_2O, 500 MHz, ppm): δ 6.71 (br, 10H), 4.11-3.56 (m, 30H), 3.53-3.23 (m, 20H), 3.03 (s, 90H), 2.43 (br, 10H), 1.12 (br, 30H). ^{13}C NMR (D_2O, 125 MHz, ppm): δ 149.8, 129.4, 116.0, 72.4, 69.9, 59.6, 53.5, 28.7, 17.8. ESI-HRMS. Calcd for $C_{105}H_{190}Br_{10}N_{10}O_{10}$ $[M-2Br]^{2+}$: 1195.4020, found 1195.4349; $[M-3Br]^{3+}$: 769.9624, found 769.9625.

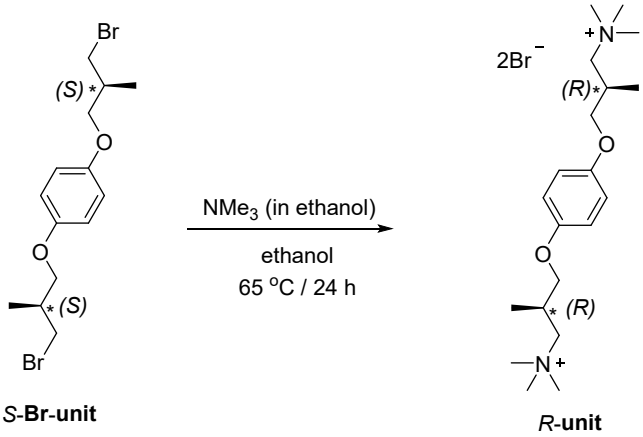

S-**Br-unit** *R*-**unit**

Scheme S2. Synthesis of *R*-**unit**.

***R*-unit.** This compound was prepared by the same procedure as *S*-**1** from *S*-**Br-unit** (57 mg, 0.15 mmol) and obtained as white solid (73 mg, yield: 98%). ^{1}H NMR (D_2O, 600 MHz, ppm): δ 6.86 (s, 4H), 3.91 (dd, J_1 = 9.9 Hz, J_2 = 4.8 Hz, 2H), 3.76-3.70 (m, 2H), 3.45 (dd, J_1 = 13.6 Hz, J_2 = 3.0 Hz, 2H), 3.19 (dd, J_1 = 13.6 Hz, J_2 = 5.8 Hz, 2H), 3.02 (br, 18H), 2.40 (br, 2H), 1.09 (d, J = 6.9 Hz, 6H). ^{13}C NMR (D_2O, 150 MHz, ppm): δ 152.6, 116.0, 71.4, 70.1, 53.3, 28.7, 17.0. ESI-HRMS. Calcd for $C_{20}H_{38}Br_2N_2O_2$ $[M-2Br]^{2+}$: 169.1461, found 169.1461.

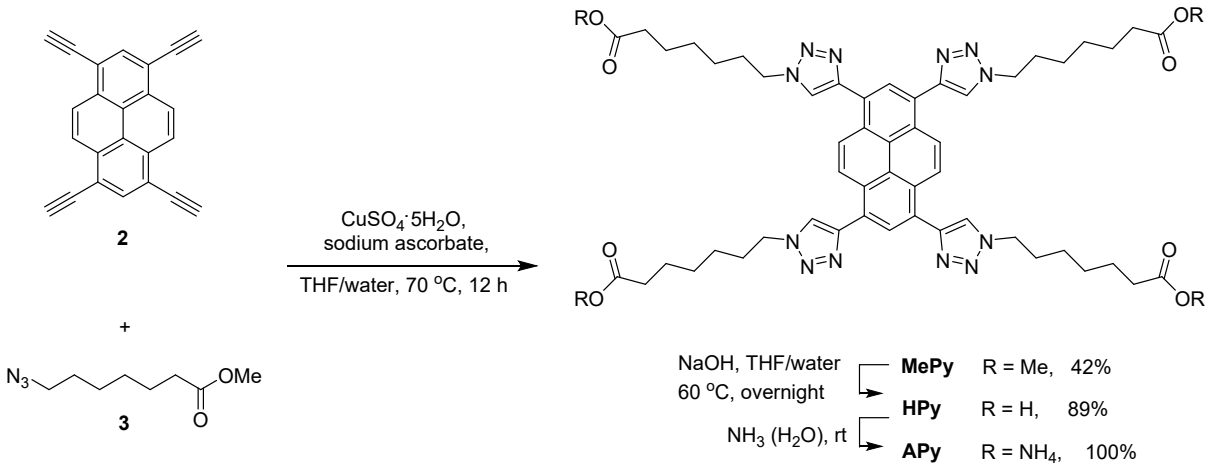

Scheme S3. Synthesis of **APy**.

Compound **2** was synthesized according to a reported procedure.[S2] ^{1}H NMR ($CDCl_3$, 400 MHz, ppm): δ 8.67 (s, 4H), 8.36 (s, 2H), 3.65, (s, 4H).

Compound **3** was synthesized according to a reported procedure.[S3] ^{1}H NMR ($CDCl_3$, 400 MHz, ppm): δ 3.65 (s, 3H), 3.24 (t, J = 6.9 Hz, 2H), 2.30 (t, J = 7.5 Hz, 2H), 1.68-1.53 (m, 4H), 1.43-1.27 (m, 4H).

MePy. To the solution of **2** (149 mg, 0.5 mmol) and **3** (463 mg, 2.5 mmol) in the mixture of THF (50 mL) and water (20 mL), $CuSO_4·5H_2O$ (499 mg, 2.0 mmol) and sodium ascorbate (792 mg, 4.0 mmol) was added. The reaction mixture was stirred vigorously at 70 ℃ for 12 hours under nitrogen atmosphere. The solution was cooled to room temperature and extracted with dichloromethane (50 mL × 3). The combined organic layers were washed with water (50 mL) and brine (50 mL), dried over anhydrous Na_2SO_4. The solvent was removed after filtration. The residual was chromatographed on silica gel column using a mixture of *n*-hexane, acetone and dichloromethane (1: 1: 0.2, v/v/v) as the mobile phase to afford yellowish solid (220 mg, yield: 42%). ^{1}H NMR ($CDCl_3$, 400 MHz, ppm): δ 8.75 (s, 4H), 8.56 (s, 2H), 8.03 (s, 4H), 4.52 (t, J = 7.2 Hz, 8H), 3.65 (s, 12H), 2.32 (t, J = 7.4 Hz, 8H), 2.12-2.01 (m, 8H), 1.72-1.62 (m, 8H), 1.52-1.37 (m, 16H). ^{13}C NMR ($CDCl_3$, 100 MHz, ppm): δ 174.1, 147.1, 128.7, 128.5, 126.0, 125.7, 123.3, 51.6, 50.5, 34.0, 30.3, 28.6, 26.4, 24.7. ESI-HRMS. Calcd for $C_{56}H_{70}N_{12}O_8$ $[M+Na]^+$: 1061.5332, found 1061.5324.

HPy. To the solution of **MePy** (150 mg, 0.144 mmol) in THF (5 mL), 5 mL of NaOH (aq., 0.4 M) was slowly added. The reaction mixture was stirred at 60 ℃ overnight. The organic solvent was evaporated under reduced pressure. HCl (aq., 1.0 M) was added dropwise until pH 1. The yellowish precipitate was collected by filtration, and washed with DI water (100 mL), dried in vacuum. The product was obtained as orange solid (126 mg, yield: 89%). ^{1}H NMR (DMSO-d_6, 500 MHz, ppm): δ 8.92 (s, 4H), 8.84 (s, 4H), 8.61 (s, 2H), 4.50 (t, J = 7.2 Hz, 8H), 2.18 (t, J = 7.4 Hz, 8H), 2.02-1.88 (m, 8H), 1.54-1.45 (m, 8H), 1.39-1.27 (m, 16H). ^{13}C NMR (DMSO-d_6, 125 MHz, ppm): δ 175.0, 146.2, 128.7, 127.9, 126.5, 126.2, 126.0, 125.3, 50.2, 34.1, 30.1,

28.5, 26.2, 24.9. ESI-HRMS. Calcd for $C_{52}H_{62}N_{12}O_8$ $[M+Na]^+$: 1005.4706, found 1005.4692.

APy. Hpy (69 mg, 0.07 mmol) was dissolved in 1 mL of ammonia (28%). The solution was stirred for 1 min, and the solvent was removed under reduced pressure. The product was obtained as yellow solid (74 mg, yield: 100%).^{1}H NMR (D_2O, 600 MHz, 353 K, ppm): δ 8.38 (s, 4H), 8.28 (s, 2H), 8.02 (s, 4H), 4.90 (t, *J* = 7.3 Hz, 8H), 2.70 (t, *J* = 7.5 Hz, 8H), 2.46-2.38 (m, 8H), 2.10-2.02 (m, 8H), 1.90-1.83 (m, 16H). ^{13}C NMR (D_2O, 150 MHz, 353 K, ppm): δ 182.5, 146.3, 127.8, 127.4, 125.0, 124.7, 124.6, 124.4, 51.2, 37.2, 30.0, 28.8, 26.3, 26.0. ESI-HRMS. Calcd for $C_{52}H_{74}N_{16}O_8$ $[M-NH_4]^-$: 987.4741, found 987.4727; $[M-2NH_4]^{2-}$: 490.2334, found 490.2329; $[M-3NH_4]^{3-}$: 326.4865, found 326.4867; $[M-4NH_4]^{4-}$: 244.6131, found 244.6154.

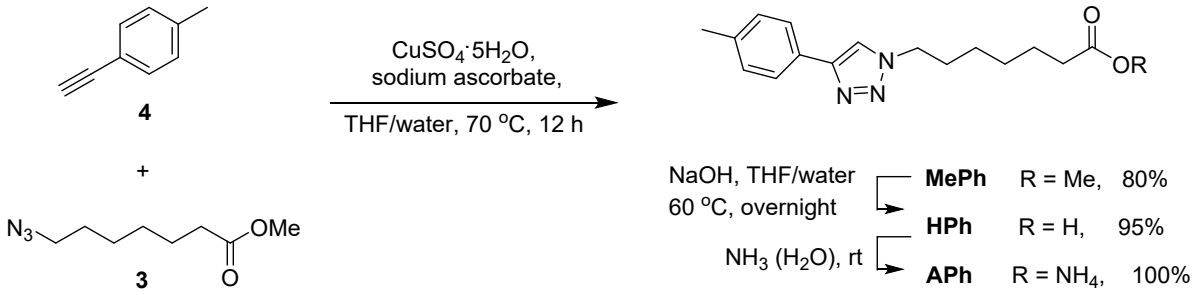

Scheme S4. Synthesis of **APh**.

MePh. To the solution of **4** (232 mg, 2.0 mmol) and **3** (185 mg, 1.0 mmol) in the mixture of THF (10 mL) and water (10 mL), $CuSO_4·5H_2O$ (250 mg, 1.0 mmol) and sodium ascorbate (396 mg, 2.0 mmol) was added. The reaction mixture was stirred vigorously at 70 ℃ for 12 hours under nitrogen atmosphere. The solution was cooled to room temperature and extracted with dichloromethane (50 mL × 3). The combined organic layers were washed with water (50 mL) and brine (50 mL), dried over anhydrous Na_2SO_4. The solvent was removed after filtration. The residual was chromatographed on silica gel column using a mixture of dichloromethane and ethyl acetate (3: 1, v/v) as the mobile phase to afford white solid (242 mg, yield: 80%). ^{1}H NMR ($CDCl_3$, 600 MHz, ppm): δ 7.70 (d, *J* = 8.1 Hz, 2H), 7.69 (s, 1H), 7.22 (d, *J* = 7.8 Hz, 2H), 4.37 (t, *J* = 7.2 Hz, 2H), 3.64 (s, 3H), 2.36 (s, 3H), 2.29 (t, *J* = 7.4 Hz, 2H), 1.97-1.90 (m, 2H), 1.64-1.58 (m, 2H), 1.39-1.33 (m, 4H). ^{13}C NMR ($CDCl_3$, 150 MHz, ppm): δ 174.1, 147.9, 138.0, 129.6, 128.0, 125.7, 119.2, 51.6, 50.3, 33.9, 30.2, 28.5, 26.2, 24.7, 21.4. APCI-HRMS. Calcd for $C_{17}H_{23}N_3O_2$ $[M+H]^+$: 302.1863, found 302.1865.

HPh. To the solution of **MePh** (226 mg, 0.75 mmol) in THF (5 mL), 5 mL of NaOH (aq., 0.4 M) was slowly added. The reaction mixture was stirred at 60 ℃ overnight. The organic solvent was evaporated under reduced pressure. HCl (aq., 1.0 M) was added dropwise until pH 1. The white precipitate was collected by filtration, and washed with DI water (100 mL), dried in vacuum. The product was obtained as orange solid (273 mg, yield: 95%). ^{1}H NMR (DMSO-d_6, 600 MHz, ppm): δ 12.00 (br, 1H), 8.51 (s, 1H), 7.72 (d, *J* = 8.1 Hz, 2H), 7.25 (d, *J* = 7.8 Hz, 2H), 4.36 (t, *J* = 7.1 Hz, 8H), 2.32 (s, 3H), 2.18 (t, *J* = 7.4 Hz, 2H), 1.88-1.80 (m, 2H), 1.52-1.44 (m, 2H), 1.35-1.21 (m, 4H). ^{13}C NMR (DMSO-d_6, 150 MHz, ppm): δ 175.0, 146.9, 137.6,

130.0, 128.6, 125.6, 121.3, 49.9, 34.1, 30.0, 28.4, 26.1, 24.8, 21.4. APCI-HRMS. Calcd for $C_{16}H_{21}N_3O_2$ $[M+H]^+$: 288.1707, found 288.1706.

APh. HPh (144 mg, 0.5 mmol) was dissolved in the mixture of 5 mL of ammonia (28%) and 5 mL of THF. The solution was stirred for 1 min, and the solvent was removed under reduced pressure. The product was obtained as white solid (151 mg, yield: 100%).^{1}H NMR (D_2O, 600 MHz, ppm): δ 8.15 (s, 1H), 7.57 (d, J = 8.2 Hz, 2H), 7.22 (d, J = 7.9 Hz, 2H), 4.32 (t, J = 6.9 Hz, 2H), 2.23 (s, 3H), 2.00 (t, J = 7.4 Hz, 2H), 1.83-1.77 (m, 2H), 1.41-1.35 (m, 2H), 1.23-1.11 (m, 4H). ^{13}C NMR (D_2O, 150 MHz, ppm): δ 184.1, 147.5, 139.3, 129.8, 126.8, 125.7, 121.9, 50.5, 37.4, 29.2, 28.0, 25.6, 25.3, 20.3. ESI-HRMS. Calcd for $C_{16}H_{24}N_4O_2$ $[M-NH_4]^-$: 286.1561, found 286.1561.

Solvent-dependent planar-chiral expression of 1

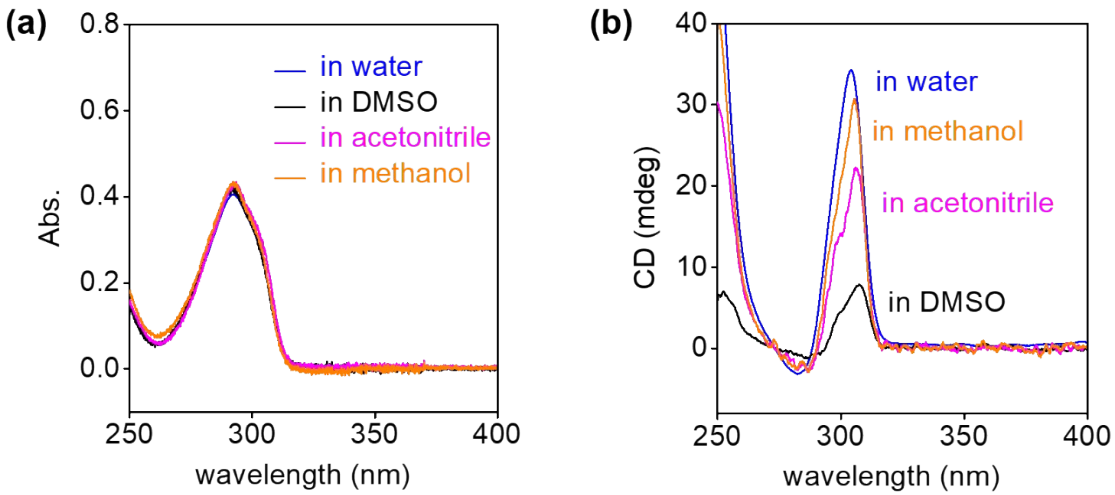

Fig. S1 (a) UV-vis and (b) CD spectra of *S*-**1** (2×10^{-5} M) in various solvents recorded at room temperature.

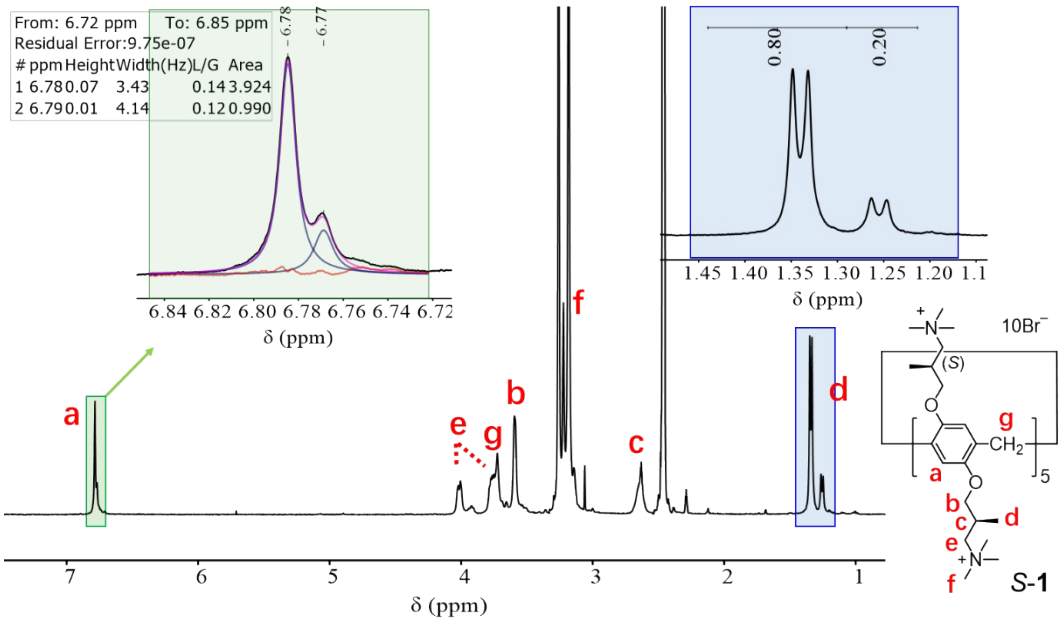

Fig. S2. ^{1}H NMR spectrum of *S*-**1** in DMSO-d_6 (400 MHz, 1 × 10^{-3} M) at room temperature. The diastereomeric excess obtained by integrating H_a and H_d was *ca*. 60%.

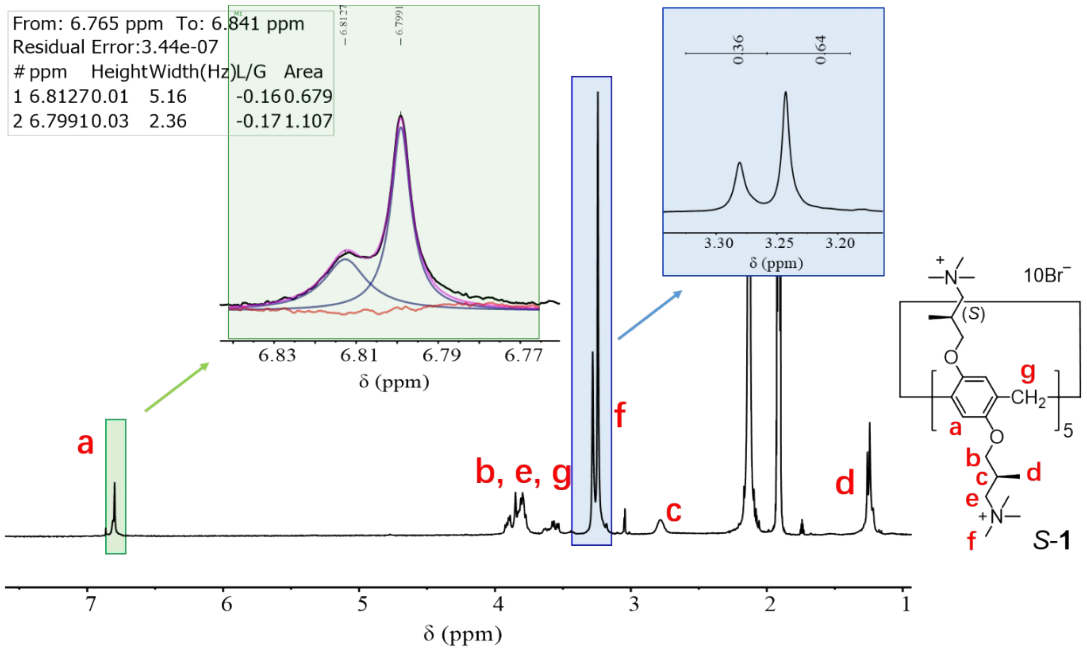

Fig. S3. ^{1}H NMR spectrum of *S*-**1** in acetonitrile-d_3 (400 MHz, saturated) at room temperature. The diastereomeric excess obtained by integrating H_a and H_f was *ca*. 26%. Acetonitrile is special for *S*-**1**, because it works as a guest molecule of the cavity of pillar[5]arenes according to previous reports.[S4] Complexation of *S*-**1** with acetonitrile could inhibit the swing of the pillar[5]arene units bridged *via* flexible methylene groups, which increased the CD intensity of *S*-**1** even with low de% value in acetonitrile (Fig. S1b).

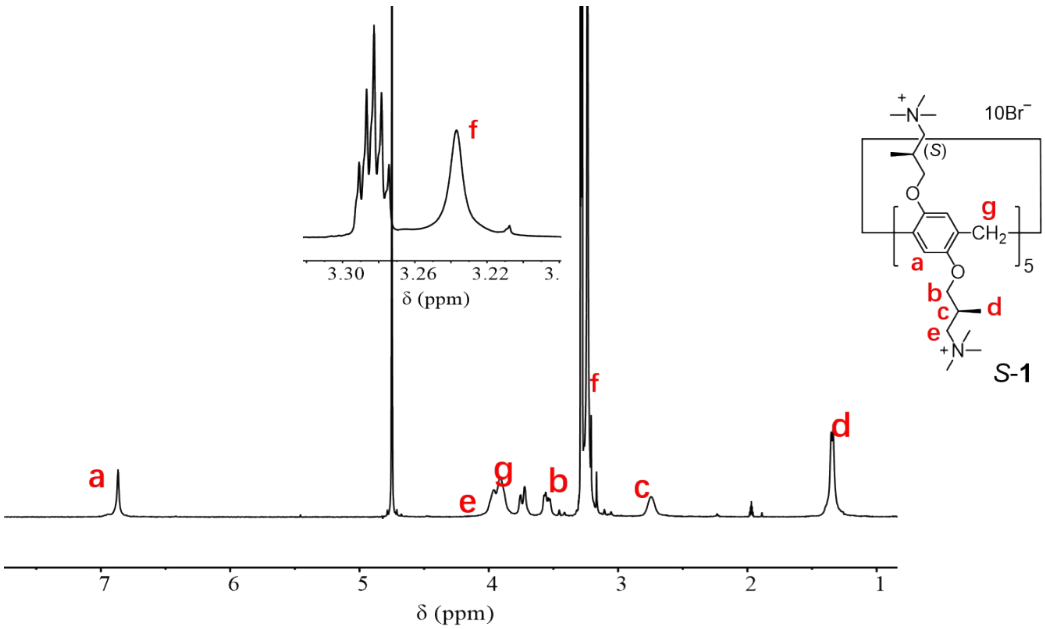

Fig. S4 ^{1}H NMR spectrum of *S*-**1** in methanol-d_4 (400 MHz, 1 × 10^{-3} M) at room temperature. Only one set of resonance signals was observed, indicating that *S*-**1** was also diastereomerically pure in methanol-d_4.

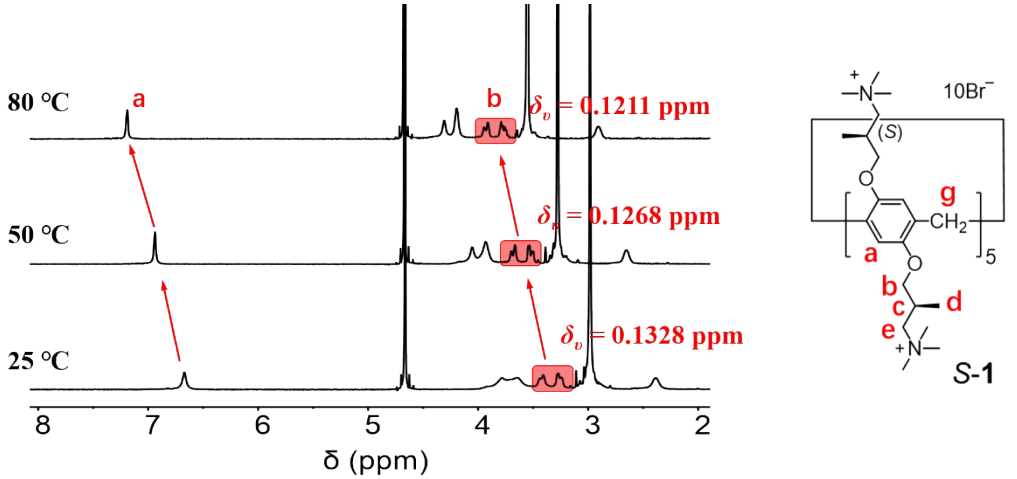

Fig. S5 Variable temperature ^{1}H NMR spectra of *S*-**1** (1 × 10^{-3} M, 400 MHz, D_2O). Upon heating, all protons became sharp and downfield shift. No split of proton H_a was observed even at 80 °C. Proton H_b, in proximity to the pillar[5]arene core of *S*-**1**, show clear AB quartet-type split even at 80 °C, indicating that the unit flip of *S*-**1** was difficult.

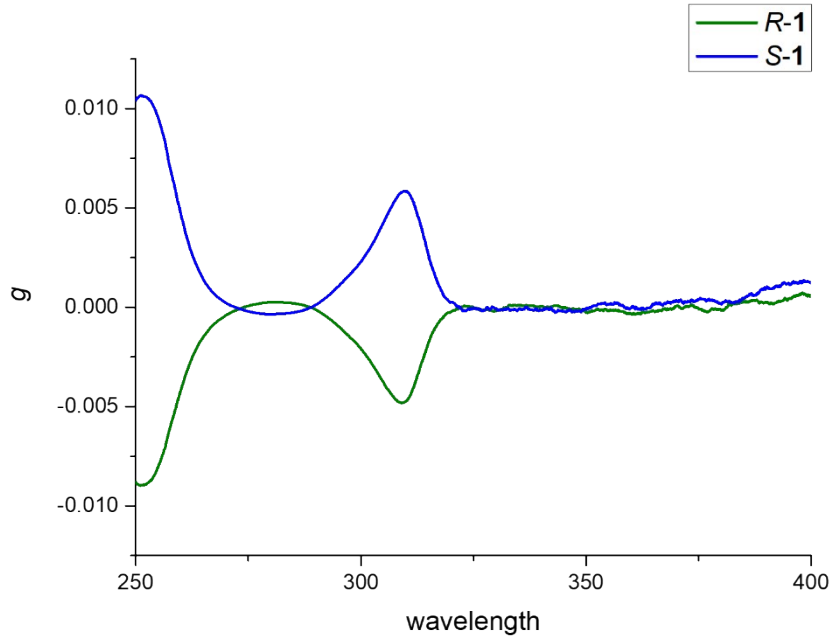

Fig. S6 Calculated dissymmetry value (*g*) of *S*-**1** and *R*-**1** in water.

Table S1. *g* values of *S*-**1** and representative pillar[5]arenes with 100% planar-chiral purity.[a]

	g (× 10^{-3})
S-**1**	5.9
5[S5]	2.9
6[S6]	7.4
7[S7]	9.9
S-**1** + **C8**	10.2

[a] The *g* values of the compounds other than *S*-**1** was calculated on the basis of the corresponding literatures.

[b] The *g* value of the complex of **C8** and *S*-**1** was calculated on the basis of Fig. S11.

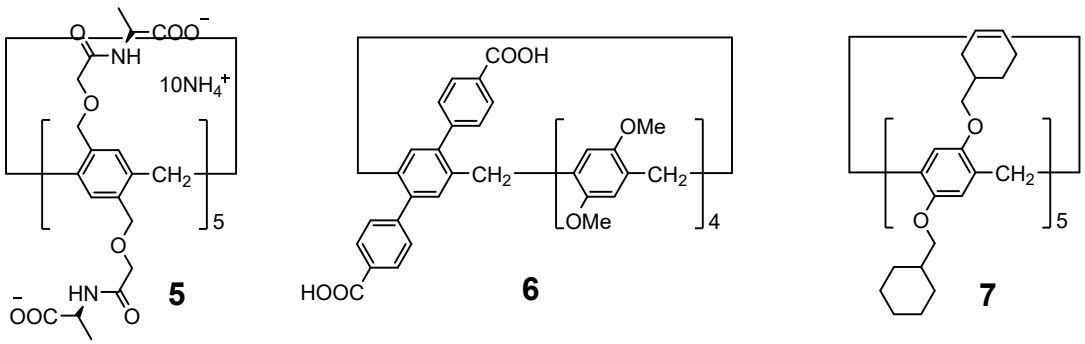

Scheme S5. Structures of planar chiral pillar[5]arenes **5**, **6**, and **7**.

Complexation of *S*-1 and *R*-1 with linear carboxylic acids C4-C9

Dicarboxylic acids **C4-C9** were able to increase the CD intensity of both *S*-**1** and *R*-**1** (Fig. 3a and S7-S12). As the length of the molecule increased, the CD intensity increased more efficiently, meaning that the equilibration reached with less dicarboxylic acids, and the final CD signal was more intensive. For example, upon addition of 200 equiv. of **C4**, the CD intensity of *S*-**1** at 304 nm increased by 1.4% (Fig. S7), while 5 equiv. of **C6** and **C8** increased the same intensity by 75% and 110%, respectively (Fig. S9 and S11).

As mentioned in the main text, *S*-**1** and *R*-**1** are diastereomerically pure in water at room temperature. Such significant increase of CD intensities of both *S*-**1** and *R*-**1** upon addition of linear dicarboxylic acids is unexpected. It is probable that the non-flipping swing of the five units of a pillar[5]arene remains allowed because of the flexibility of bridging methylene groups of **1**, although the flip is inhibited at room temperature. This was revealed by the relative broad signals of both *S*-**1** and *R*-**1** in ^{1}H NMR spectra. The swing of pillar[5]arene units would prevent the full expression of CD signals. Upon addition of dicarboxylic acids, the swing of pillar[5]arene units was inhibited by complexation, and the CD intensity of **1** increased subsequently. Because **1** was diastereomerically pure in water, the binding constants (K_a) between dicarboxylic acids and **1** could be determined by CD titration (Table S2). In case of **C4**, the K_a is too small to be determined. The K_a of the complexes between *S*-**1** and **C6** and **C8** are $(3.66 \pm 0.44) \times 10^4$ M^{-1} and $(6.30 \pm 1.02) \times 10^5$ M^{-1}, respectively. It is apparent that the binding affinity increased as the length of the guest molecule increased. The association constants were summarized in Table S2.

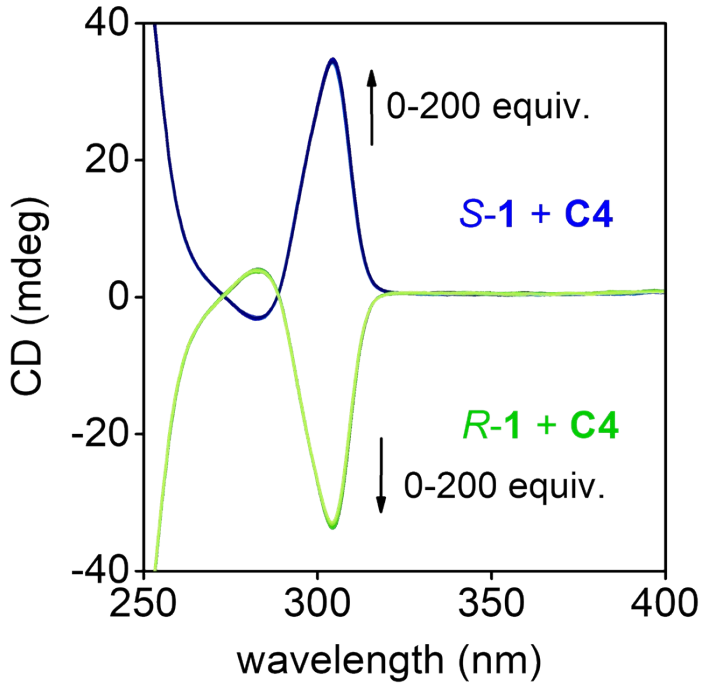

Fig. S7 CD spectra of *S*-**1** and *R*-**1** (2×10^{-5} M) in water upon addition of **C4**.

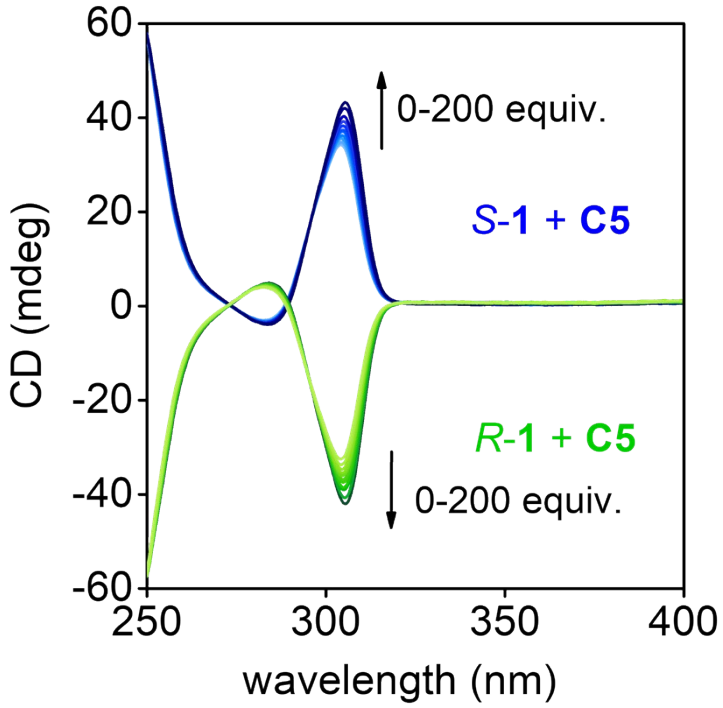

Fig. S8 CD spectra of *S*-**1** and *R*-**1** (2×10^{-5} M) in water upon addition of **C5**.

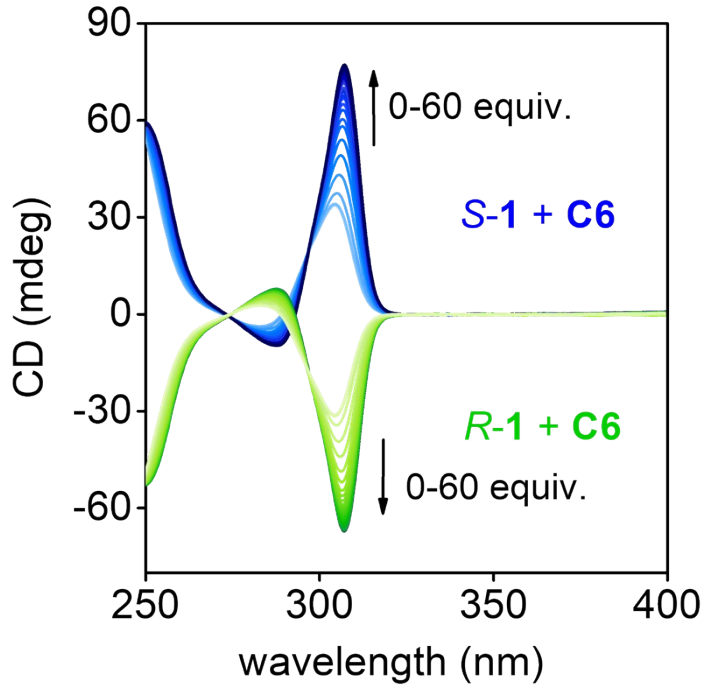

Fig. S9 CD spectra of *S*-**1** and *R*-**1** (2×10^{-5} M) in water upon addition of **C6**.

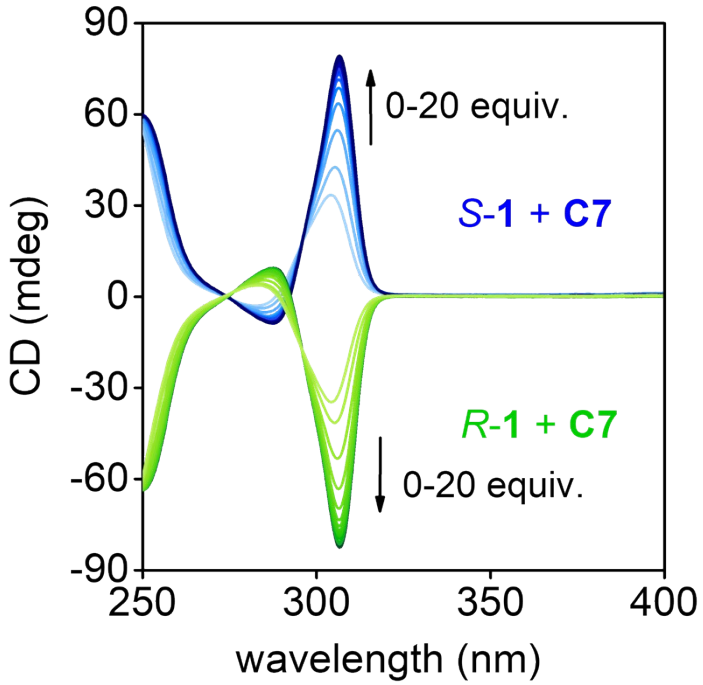

Fig. S10 CD spectra of *S*-**1** and *R*-**1** (2×10^{-5} M) in water upon addition of **C7**.

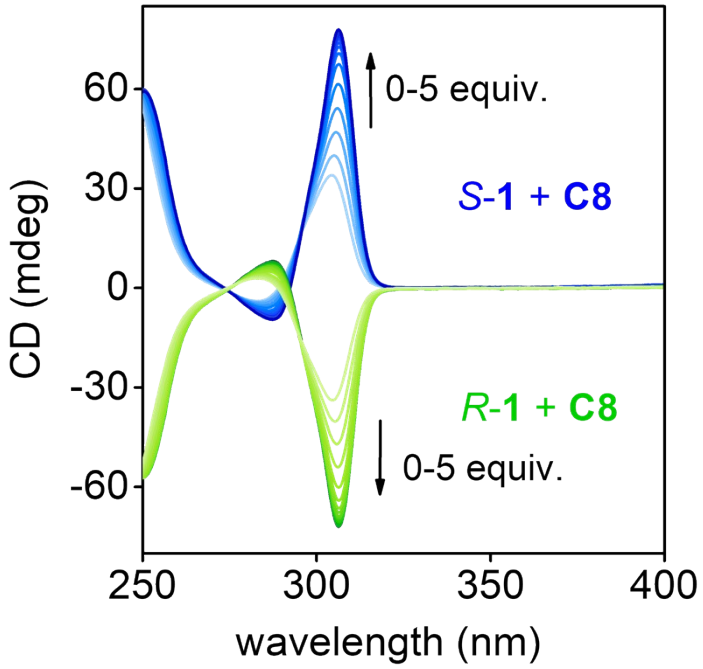

Fig. S11 CD spectra of *S*-**1** and *R*-**1** (2×10^{-5} M) in water upon addition of **C8**.

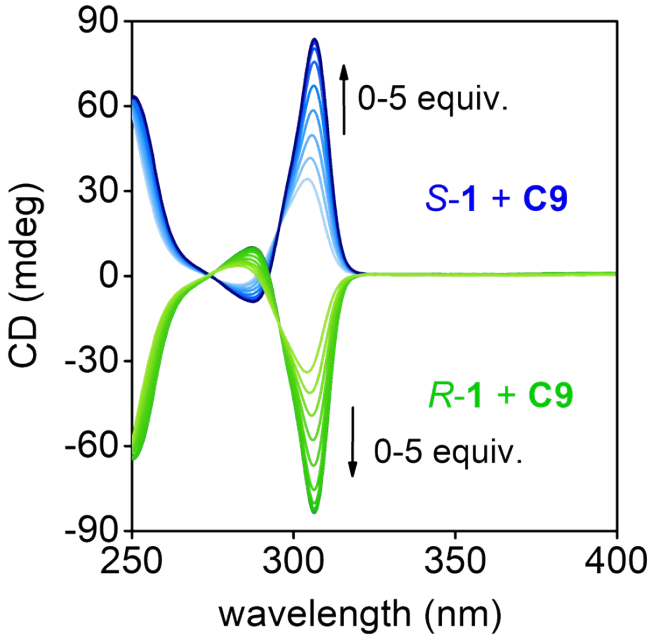

Fig. S12 CD spectra of *S*-**1** and *R*-**1** (2×10^{-5} M) in water upon addition of **C9**.

Table S2. Association constants (K_a) between dicarboxylic acids and **1**.[a]

	K_a ($\times 10^4$ M^{-1})	
	S-**1**	*R*-**1**
C4	-[b]	-[b]
C5	-[b]	-[b]
C6	3.66 ± 0.44	3.41 ± 0.43
C7	11.0 ± 1.3	7.84 ± 1.18
C8	63.0 ± 10.2	53.2 ± 8.0
C9	143 ± 40	130 ± 41

[a]K_a was calculated by fitting the CD change at 304 nm upon titration at 25 °C.
[b]Too small to be determined by CD titration.

To investigate the binding mode between **1** and **C4**-**C9**, the ^{1}H NMR spectra of *S*-**1** upon addition of dicarboxylic acids were measured. Upon addition of 20 equiv. of **C4**, no chemical shift change was observed for all protons on *S*-**1**, suggesting that the complexation between **C4** and *S*-**1** was too weak to be detected by NMR titration (Fig. S13). Differently, all protons of *S*-**1** shifted downfield and became sharper upon addition of **C6** (Fig. S14). Furthermore, two new proton signals of **C6** appeared at -0.17 ppm and -1.60 ppm. These observations indicated that **C6** threaded through the cavity of *S*-**1** and a complex was formed in D_2O. The complex between **C8** and *S*-**1** was more stable kinetically and thermodynamically. When 0.5 equiv. of **C8** was added in the solution of *S*-**1**, clear signals of complex (H_a'-H_g') and free components (H_a-H_g) were observed in ^{1}H NMR spectrum (Fig. S15), suggesting that the exchange speed between complex and free components are slower than the NMR time scale. This slow exchange led to the

high degree of CD increase of *S*-**1**. The mixture of **C8** and *S*-**1** in 1:1 ratio shows only the signals of complex in ^{1}H NMR spectrum, indicating a strong binding.

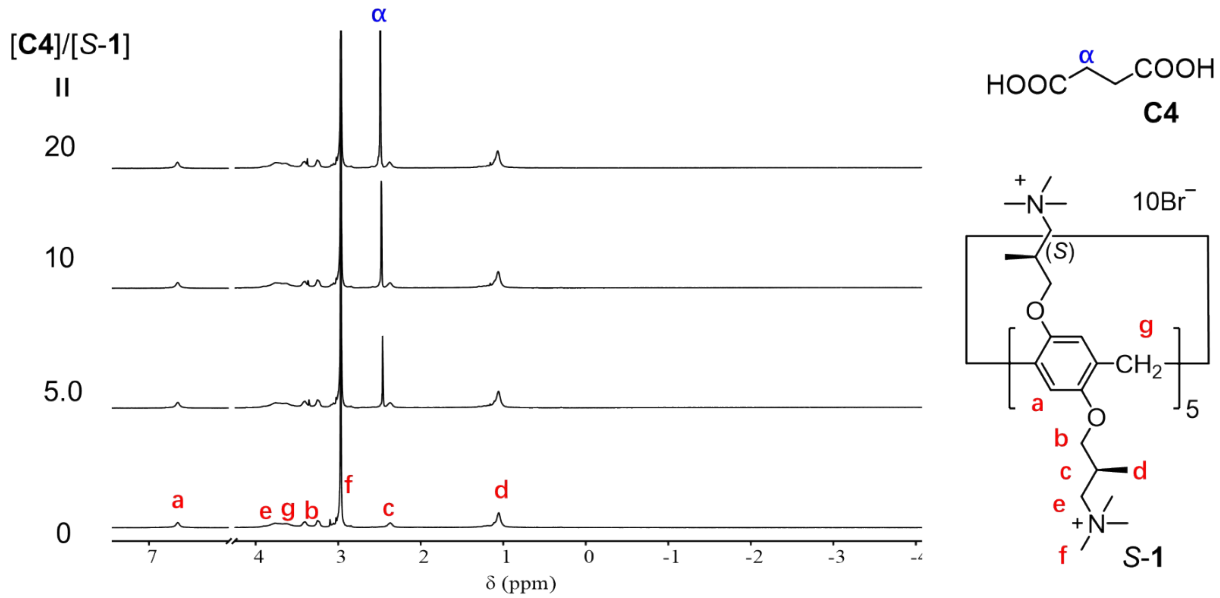

Fig. S13 Partial ^{1}H NMR spectra of *S*-**1** (5×10^{-4} M, 600 MHz, D_2O) upon addition of **C4** at room temperature. No chemical shift change of H_a-H_g was observed.

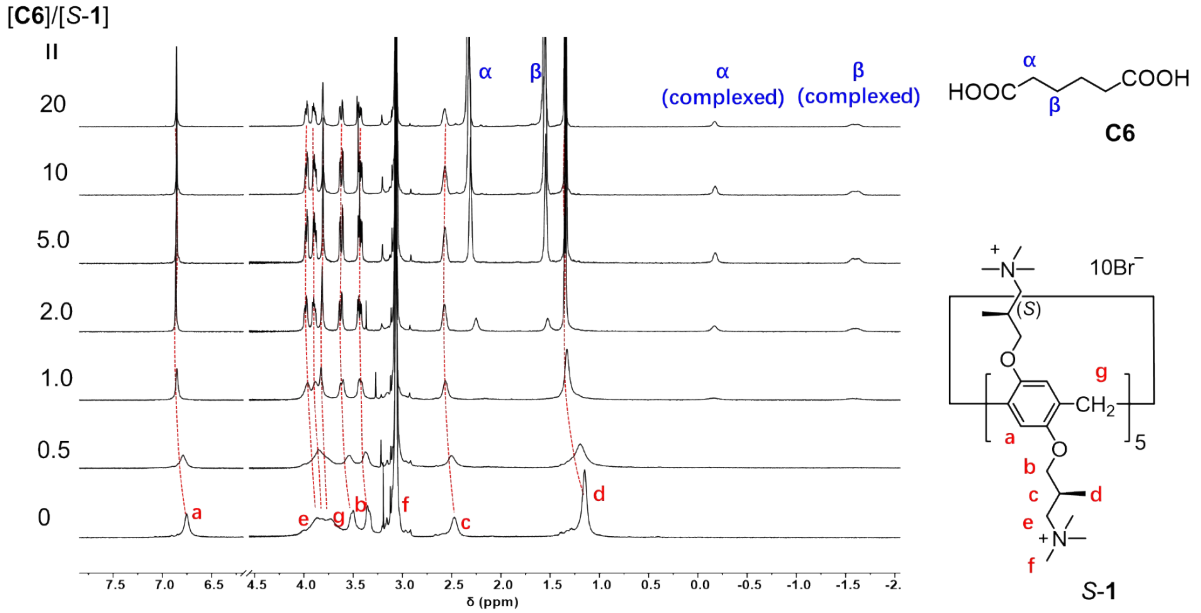

Fig. S14 Partial ^{1}H NMR spectra of *S*-**1** (5×10^{-4} M, 400 MHz, D_2O) upon addition of **C6** at room temperature. All protons on *S*-**1** shift downfield.

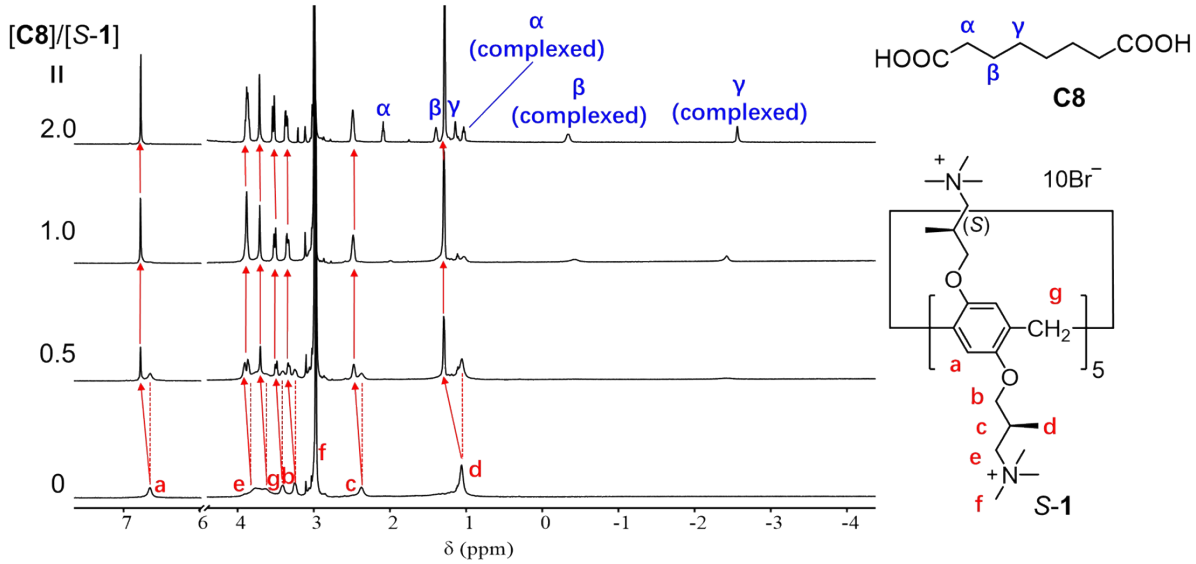

Fig. S15 Partial ^{1}H NMR spectra of *S*-**1** (5×10^{-4} M, 600 MHz, D_2O) upon addition of **C8** at room temperature. All protons on *S*-**1** split to two sets upon addition of 0.5 equiv. of **C8**. When over 1 equiv. of **C8** was added, signals ascribed to free *S*-**1** disappeared.

Assembly of APy in water

The fluorescent spectra of **APy** showed a drastic concentration dependent spectral change (Fig. S16 and S17). At low concentrations, the fluorescence maximum was clearly observed at *ca*. 426 nm, corresponding to the emission of monomeric **APy**. As concentration increased, a new fluorescence band emerged at *ca*. 530 nm and gradually red-shift. This indicated the formation of the π-oligomer of **APy** and suggested the high molecular aggregation ability of **APy** in water. Actually, the fluorescence band at *ca*. 530 nm can be observed even at very low concentration (e.g., 1×10^{-7} M). However, it is clear that the monomeric emission at *ca*. 426 nm significantly decreased at concentrations above 2×10^{-5} M (Fig. S17b), while the oligomeric emission at *ca*. 530 nm kept constant, resulting in sharp increase of the ratio of fluorescence intensities I_{531}/I_{426}. This implied that the aggregates of **APy** were dominant above 2×10^{-5} M in water, which was revealed by concentration-dependent and temperature variable ^{1}H NMR measurements (Fig. S18 and S19).

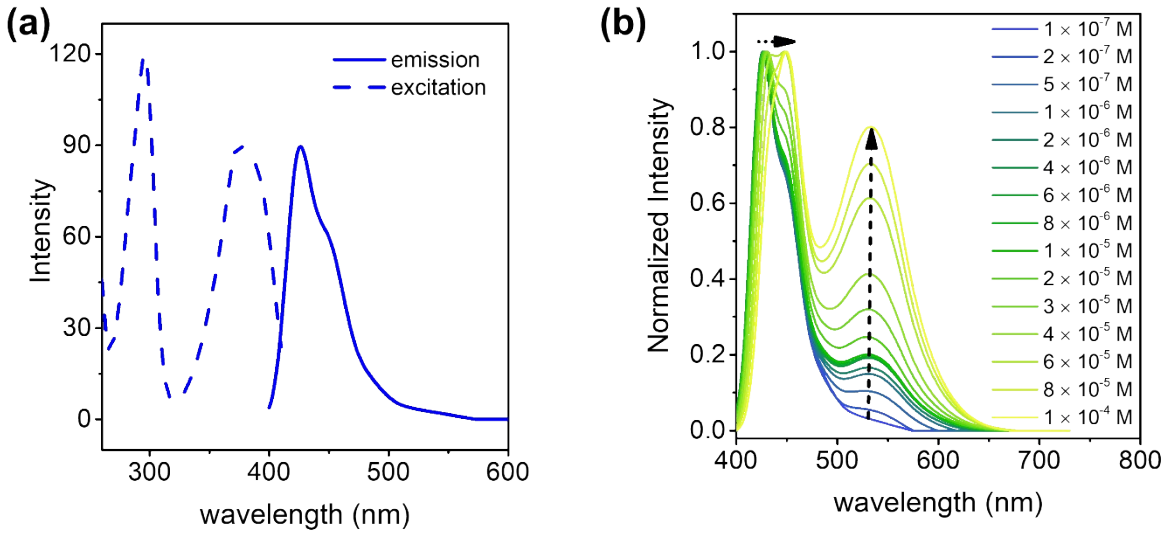

Fig. S16 (a) Excitation (λ_{em} = 426 nm) and emission (λ_{ex} = 385 nm) spectra of **APy** in water at 1×10^{-7} M. (b) Normalized fluorescence spectra of **APy** in water at various concentrations. All spectra were recorded at room temperature.

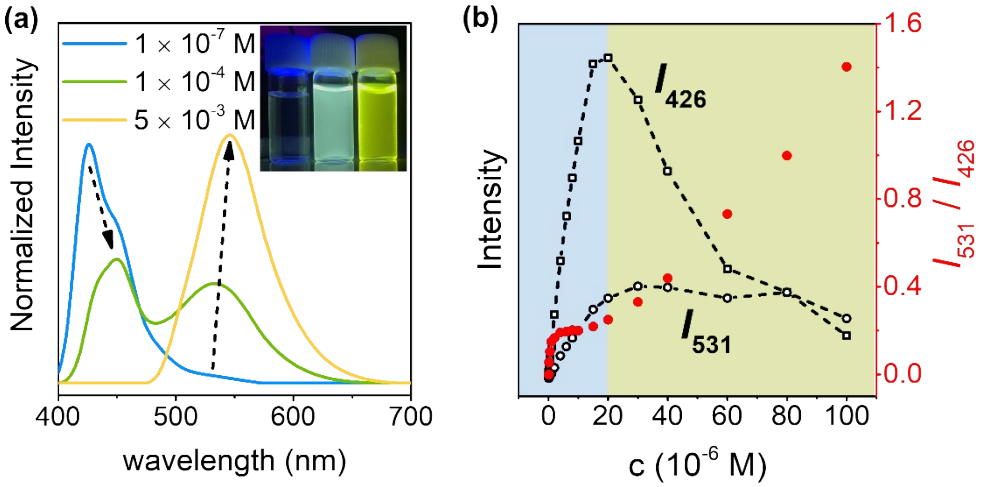

Fig. S17 (a) Fluorescence spectra (λ_{ex} = 385 nm) of **APy** at *c*-range from 1×10^{-7} to 5×10^{-3} M. Inset: Images under UV light (365 nm) of **APy** at various concentrations: 1×10^{-7}, 1×10^{-4} and 5×10^{-3} M (from left to right). (b) Plots of fluorescence intensity at 426 nm and 531 nm, and their ratio against the concentration of **APy**.

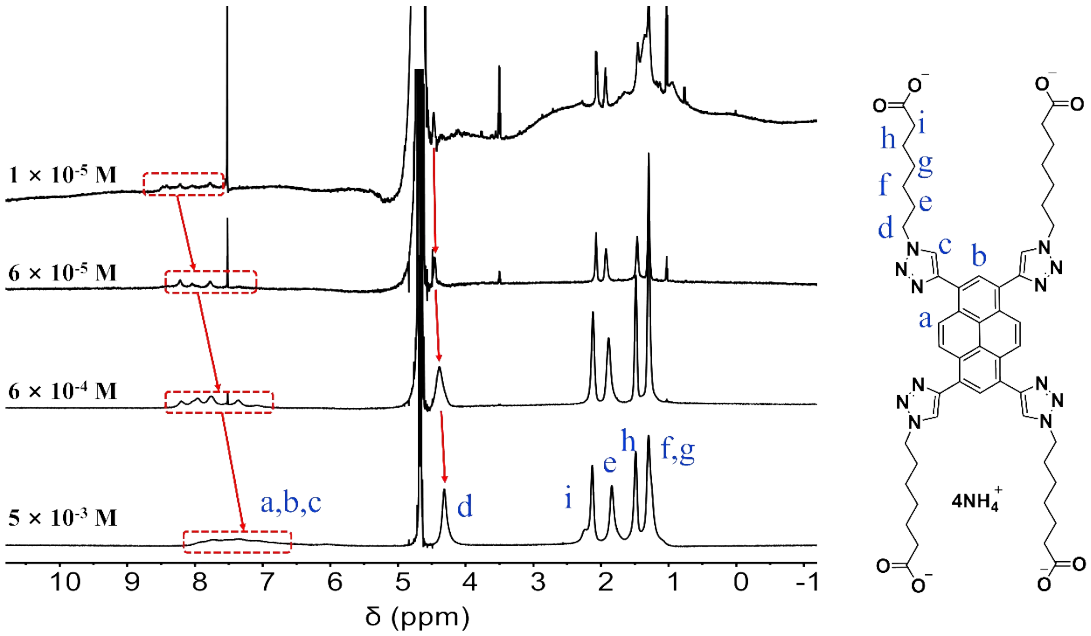

Fig. S18 ^{1}H NMR spectra of **APy** (600 MHz, D_2O) at various concentrations. All spectra were recorded at room temperature. Under all tested conditions, the resonances of pyrene (i.e., protons a and b) and triazole (i.e., proton c) moieties became broadening and splitting, indicating the stacking between the π-conjugated parts of **APy** at all tested concentrations. Moreover, the signals of protons a, b, c and d gradually upfield shift as concentration increasing, which suggests that larger assemblies formed. In contrast, protons e-f do not show clearly shift, because the interactions of the periphery of **APy** are relative weak.

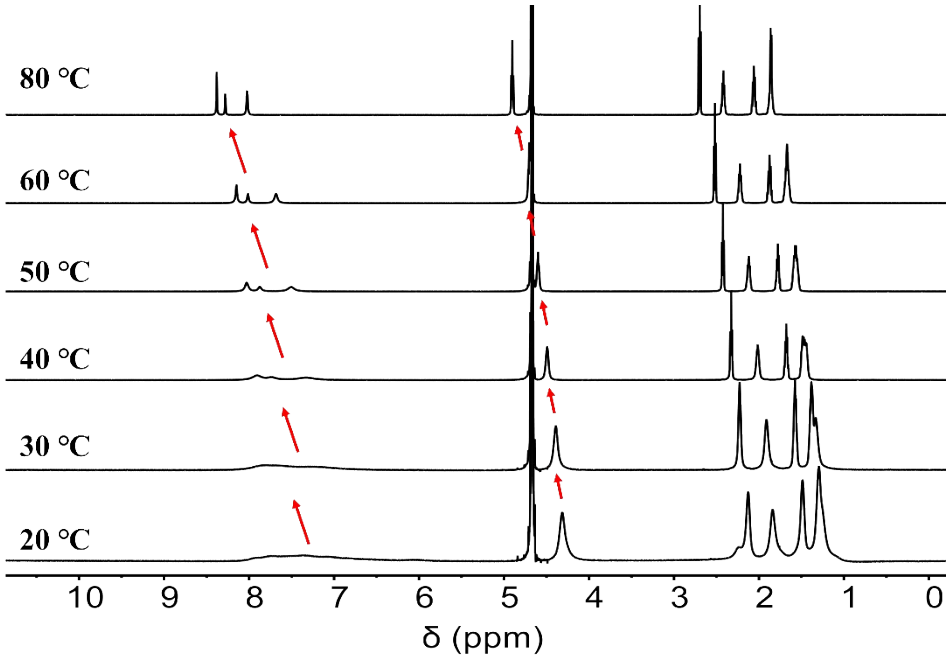

Fig. S19 Variable temperature ^{1}H NMR spectra of **APy** (5×10^{-3} M, 600 MHz, D_2O). Upon heating, the stacking of the π-conjugated parts of **APy** weakened, and the signals showed downfield shift and became sharp, indicating decomposition of the assemblies of **Apy**. At 80 °C, only signals of monomeric **Apy** were observed.

Two-step complexation of APy with 1 in water

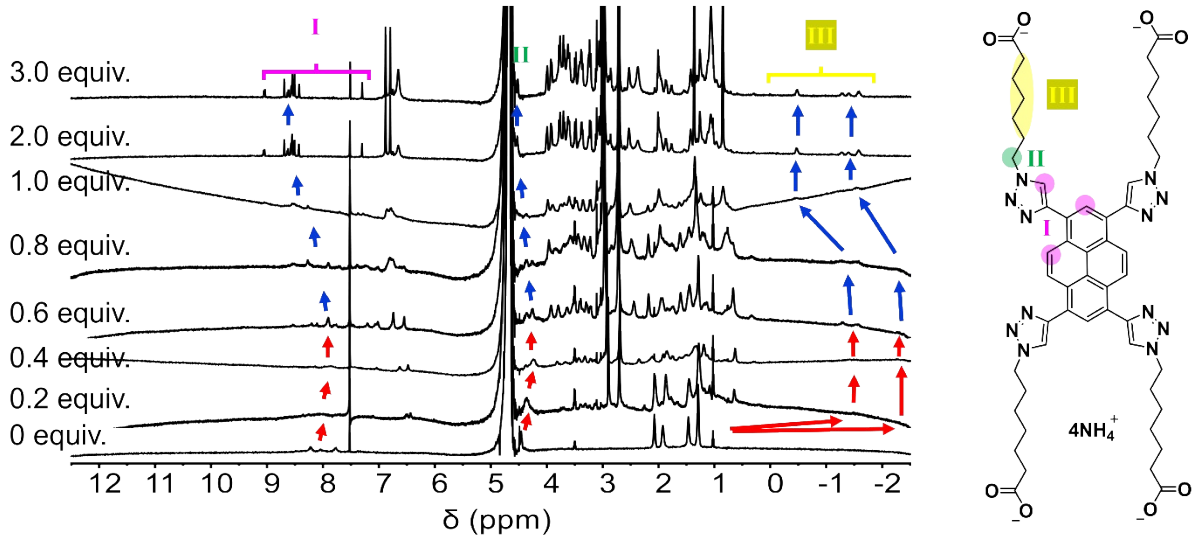

Fig. S20 ^{1}H NMR spectra of **APy** (6×10^{-5} M, 600 MHz, D_2O) upon addition of 0.2, 0.4, 0.8, 1.0, 2.0 and 3.0 equiv. of *S*-**1** (from bottom to top). A two-step complexing process was clearly observed. The initial broadening and upfield shift of all resonance signals (illustrated by red arrows) suggested assembly of **APy** upon addition of less than 0.6 equiv. of *S*-**1**. As further adding *S*-**1**, subsequent sharpening and down-field shift of resonances was observed, suggesting the disassembly process. In especial, the signals corresponding to the linear alkyl chains of **APy** (protons III) drastically upfield shift to around -1 to -2 ppm, indicating strong shielding effect due to inclusion of these protons by the cavity of *S*-**1**.

In order to clearly understand the binding between **1** and **APy**, complexation between **1** and **APh**, the unit model of **APy**, was also investigated by CD titration and NMR measurements (Fig. S21-S24). In the NMR spectra, the resonances of free **APh** and complexed **APh** were also clearly separated, indicating a slower exchange than the NMR scale. This was similar to the observations of **C8**. With the same alkyl chain between the two ends as **C8**, **APh** possesses similar association constants with *S*-**1** and *R*-**1**. The binding constants of *S*-**1** and *R*-**1** with **APh** were determined to be $(8.02 \pm 2.41) \times 10^5$ M^{-1} and $(1.10 \pm 0.30) \times 10^6$ M^{-1}, respectively.

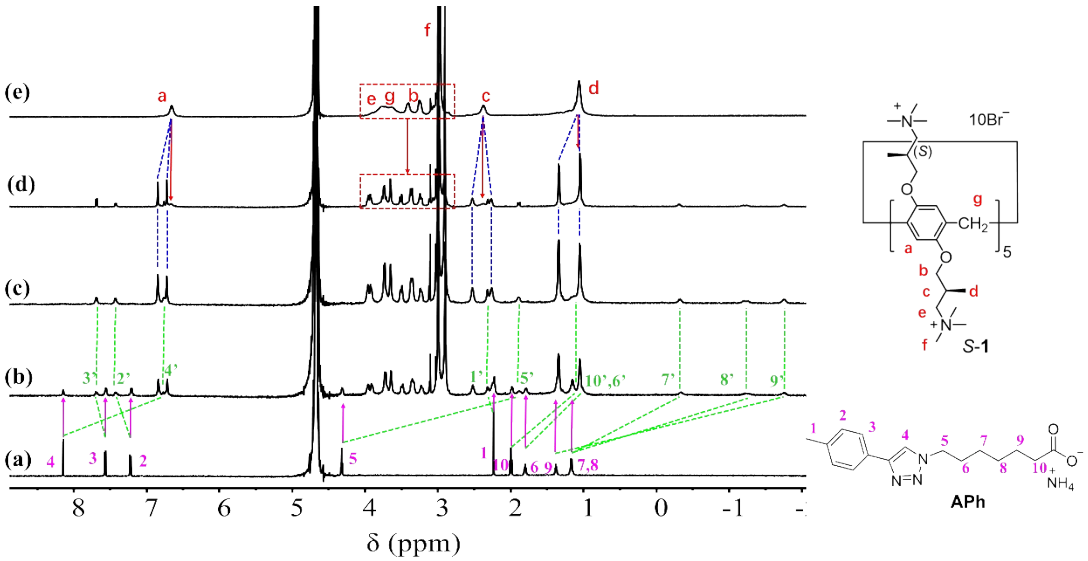

Fig. S21 ^{1}H NMR spectra of **APh** (2.5×10^{-4} M, 600 MHz, D_2O) upon addition of *S*-**1** at room temperature. From (a) to (d), 0, 0.5, 1.0 and 2.0 equiv. of *S*-**1** were added, respectively. (e) ^{1}H NMR spectra of *S*-**1** (5×10^{-4} M, 600 MHz, D_2O). (b) All protons on **APh** split to two sets upon addition of 0.5 equiv. of *S*-**1**, indicating that the exchange between complexed and free **APh** was slower than the NMR time scale. Therefore, relative stable complex formed between **APh** and *S*-**1**. (c) As 1 equiv. of *S*-**1** was added, signals ascribed to free **APh** disappeared, indicating that the complexation between **APh** and *S*-**1** was strong. (d) By complexation, peaks of *S*-**1** also split to two sets due to the asymmetric structure of **APh**. It is clear that the binding between *S*-**1** and **APh** was strong, and the alkyl chain of **APh** was deeply included in the cavity of *S*-**1** as complexation.

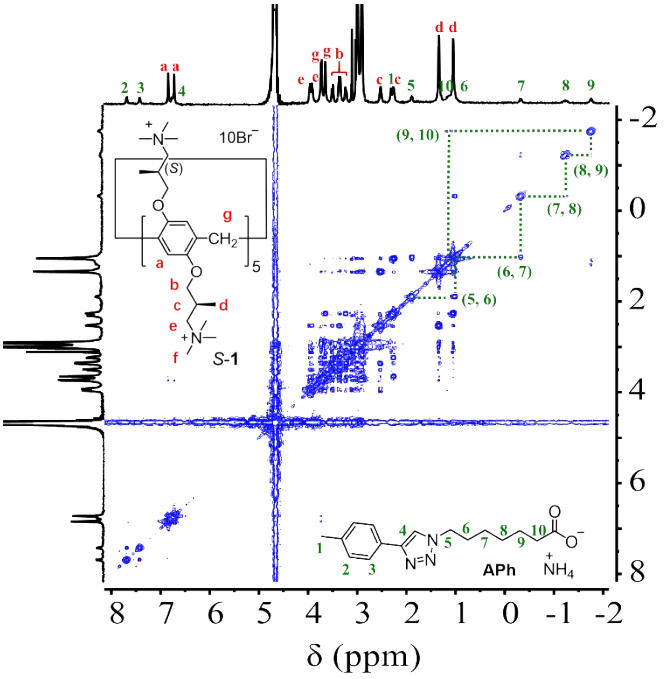

Fig. S22 2D COSY spectrum (600 MHz, D_2O) of the 1:1 mixture of **APh** (2.5×10^{-4} M) and *S*-**1** (2.5×10^{-4} M). Only the resonance of the complex was observed. The correlation between the complexed **APh** protons was shown.

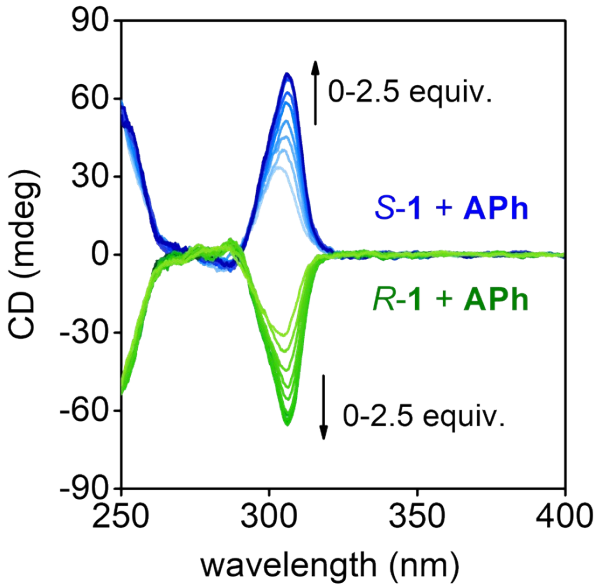

Fig. S23 CD spectra of *S*-**1** and *R*-**1** (2×10^{-5} M) in water upon addition of **APh**.

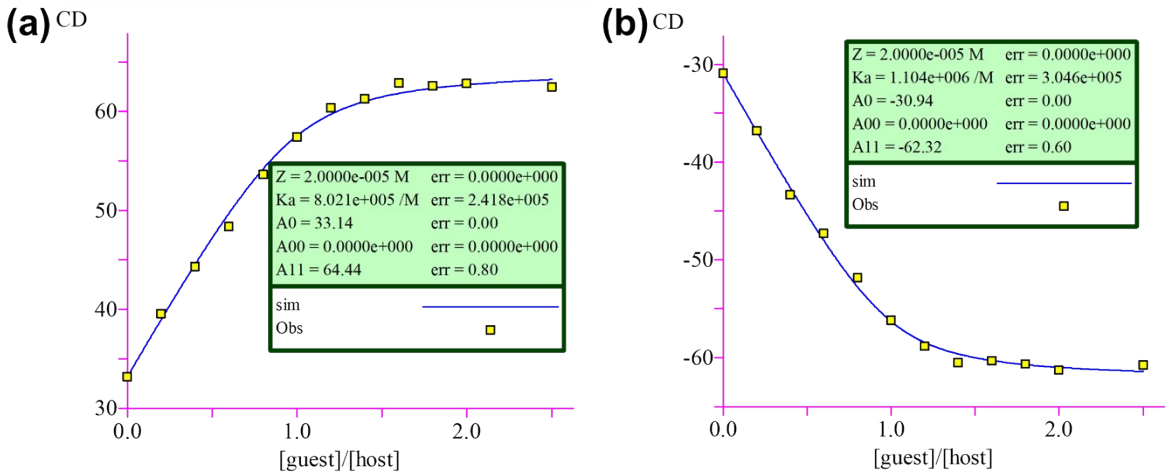

Fig. S24 Non-linear curve-fittings for CD intensity at 304 nm of (a) *S*-**1** and (b) *R*-**1** upon addition of **APh**. The data was taken from Fig. S23. The binding constants of *S*-**1** and *R*-**1** with **APh** were determined to be $(8.02 \pm 2.41) \times 10^5$ M^{-1} and $(1.10 \pm 0.30) \times 10^6$ M^{-1}, respectively.

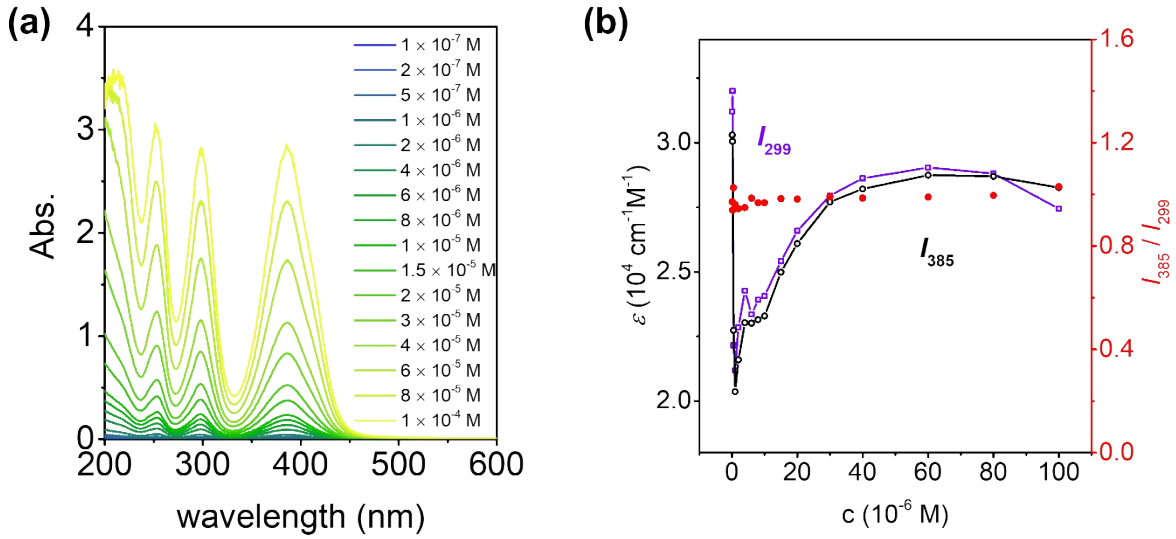

Fig. S25 (a) UV-vis spectra of **APy** in water at *c*-range from 1×10^{-7} to 1×10^{-4} M. (b) Plots of molar absorption coefficient (ε) at 299 nm and 385 nm, and their ratio against the concentration of **APy**. All spectra were recorded at room temperature.

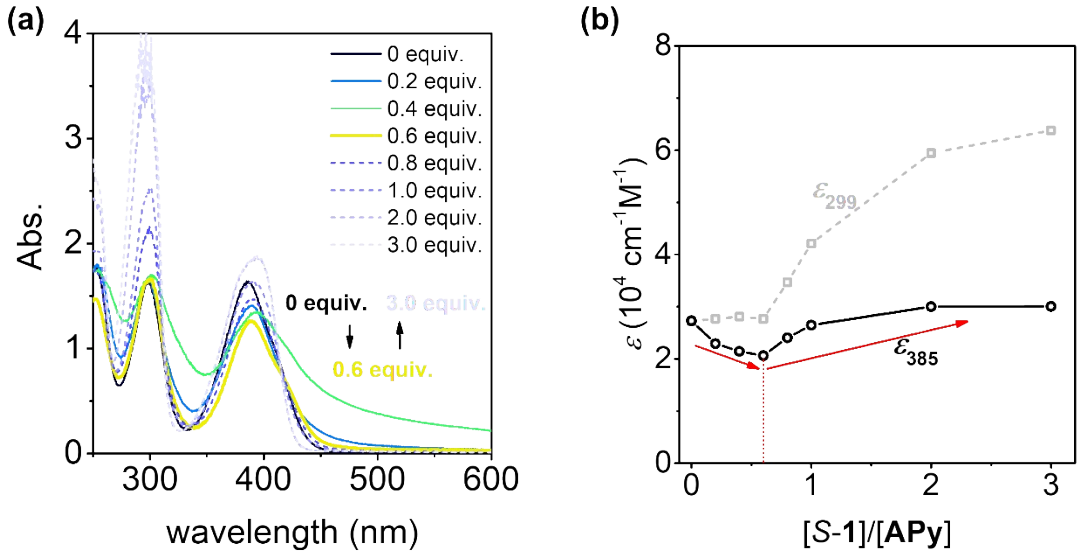

Fig. S26 UV-vis spectra of **APy** (6×10^{-5} M) upon addition of *S*-**1**. (b) Plots of ε at 299 nm and 385 nm against the ratio of *S*-**1** and **APy**. All spectra were recorded at room temperature. The absorption at 299 nm partly overlapped with *S*-**1**, so it is not suitable for analyzing the intensity change upon titration. The absorption at 385 nm clearly showed the two-step process.

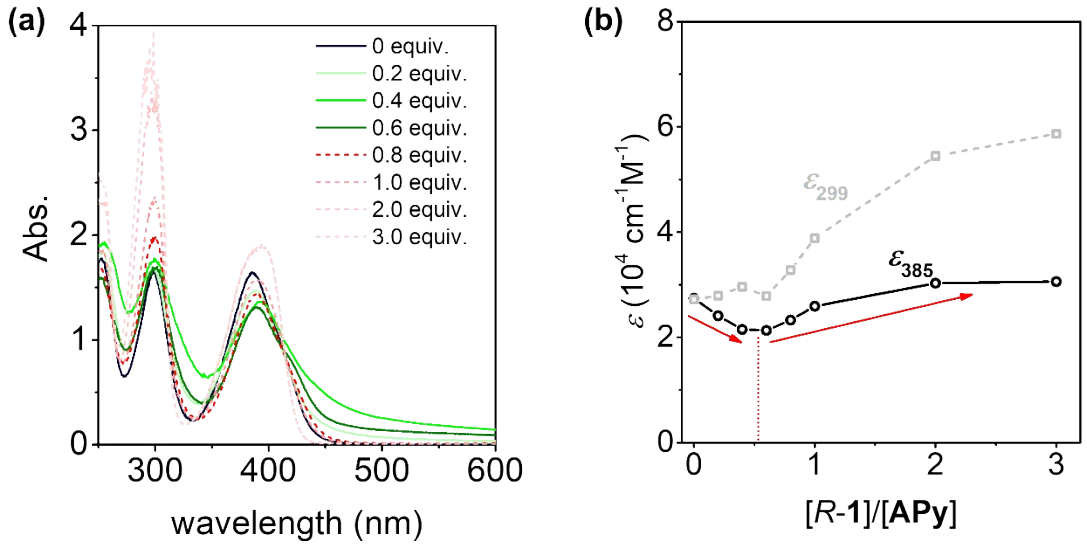

Fig. S27 UV-vis spectra of **APy** (6×10^{-5} M) upon addition of *R*-**1**. (b) Plots of ε at 299 nm and 385 nm against the ratio of *R*-**1** and **APy**. All spectra were recorded at room temperature. The absorption at 299 nm partly overlapped with *R*-**1**, so it is not suitable for analyzing the intensity change upon titration. The absorption at 385 nm clearly showed the two-step process.

Chirality transfer from chiral 1 to APy

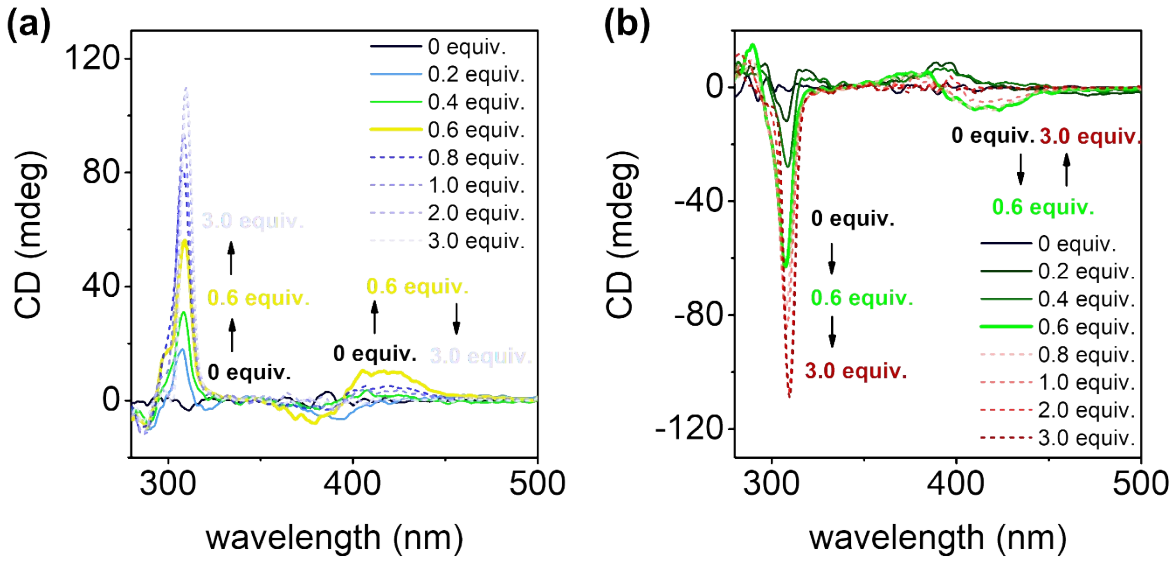

Fig. S28 CD spectra of **APy** (6×10^{-5} M) upon addition of (a) *S*-**1** and (b) *R*-**1**. All spectra were recorded at room temperature.

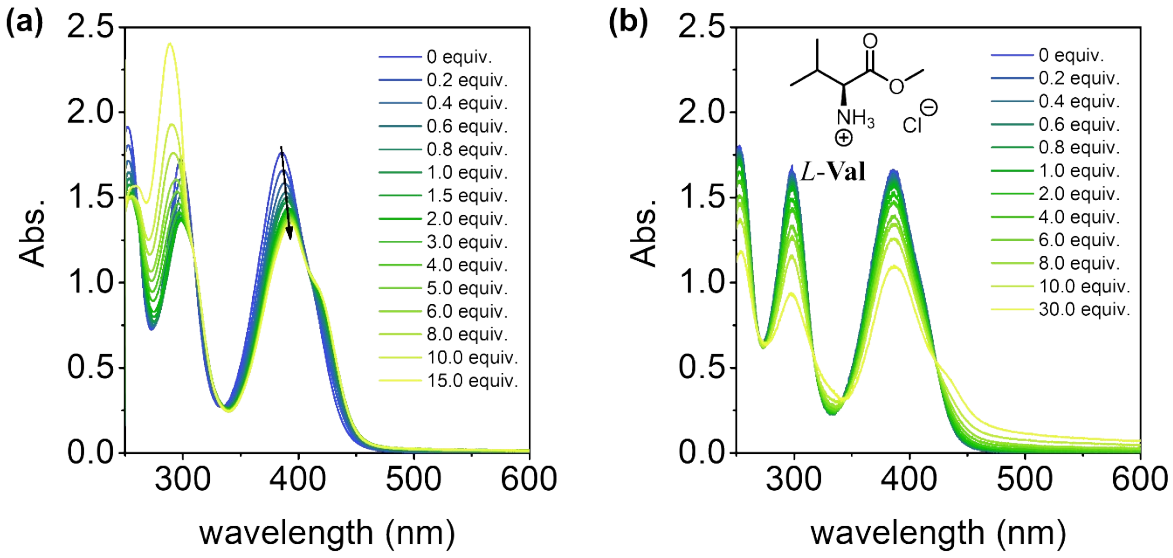

Fig. S29 UV-vis spectra of **APy** (6×10^{-5} M) upon addition of (a) *R*-**unit** and (b) *L*-**Val**. All spectra were recorded at room temperature.

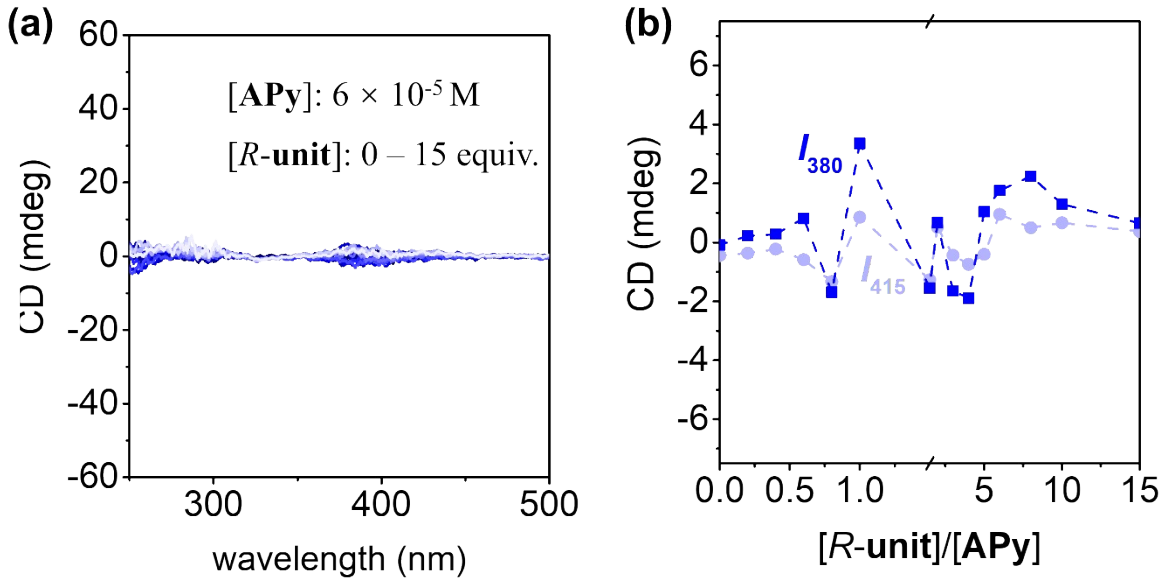

Fig. S30 (a) CD spectra of **APy** (6×10^{-5} M) upon addition of *R*-**unit**. (b) Plots of CD at 415 nm and 380 nm of **APy** (6×10^{-5} M) upon addition of *R*-**unit**. All spectra were recorded at room temperature. Only random and weak CD signals were observed upon titration.

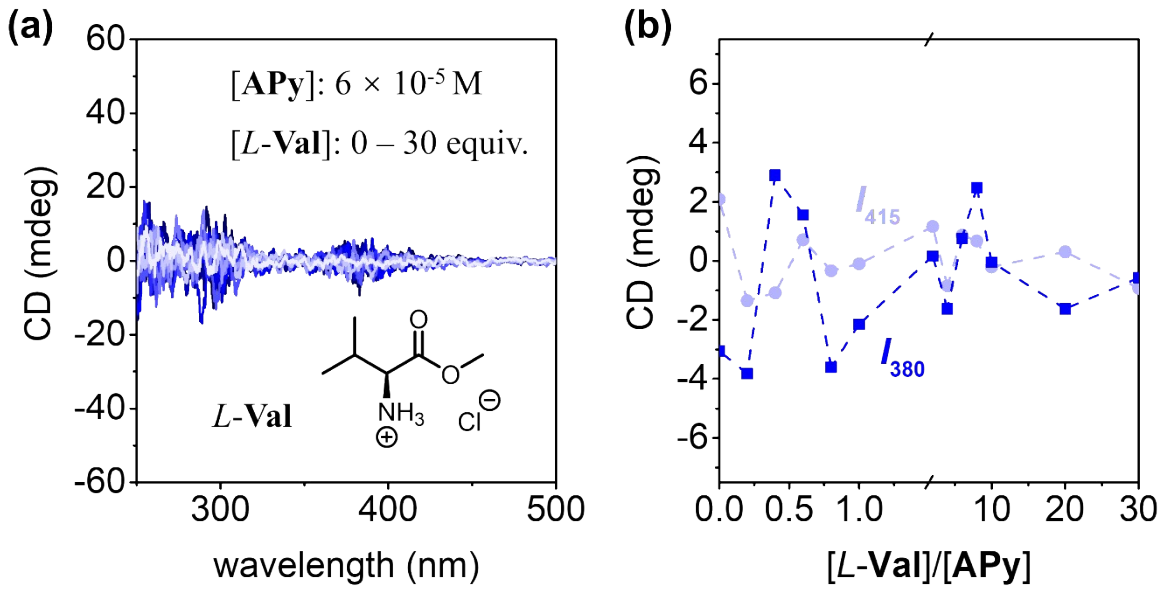

Fig. S31 (a) CD spectra of **APy** (6×10^{-5} M) upon addition of *L*-**Val**. (b) Plots of CD at 415 nm and 380 nm of **APy** (6×10^{-5} M) upon addition of *L*-**Val**. All spectra were recorded at room temperature. Only random and weak CD signals were observed upon titration.

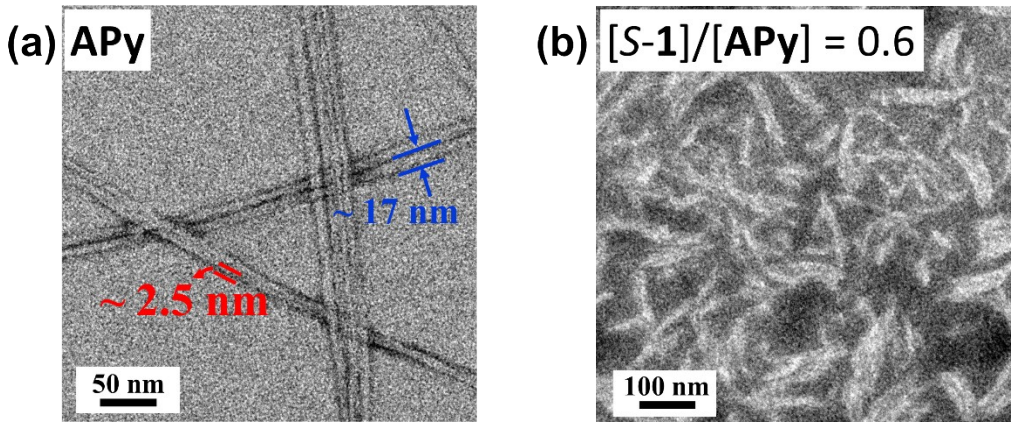

Fig. S32 TEM images of (a) **Apy**, and (b) the mixture of **APy** with *S*-**1**: [*S*-**1**]/[**APy**] = 0.6.

Assembly and disassembly of APy triggered by chiral 1

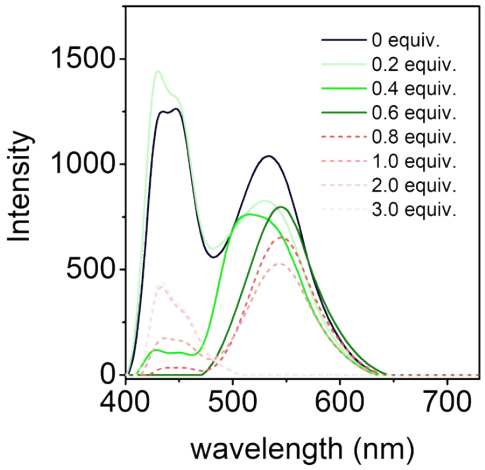

Fig. S33 (a) Fluorescence spectra (λ_{ex} = 385 nm) of **APy** (6 × 10^{-5} M) upon addition of *R*-**1**. All spectra were recorded at room temperature.

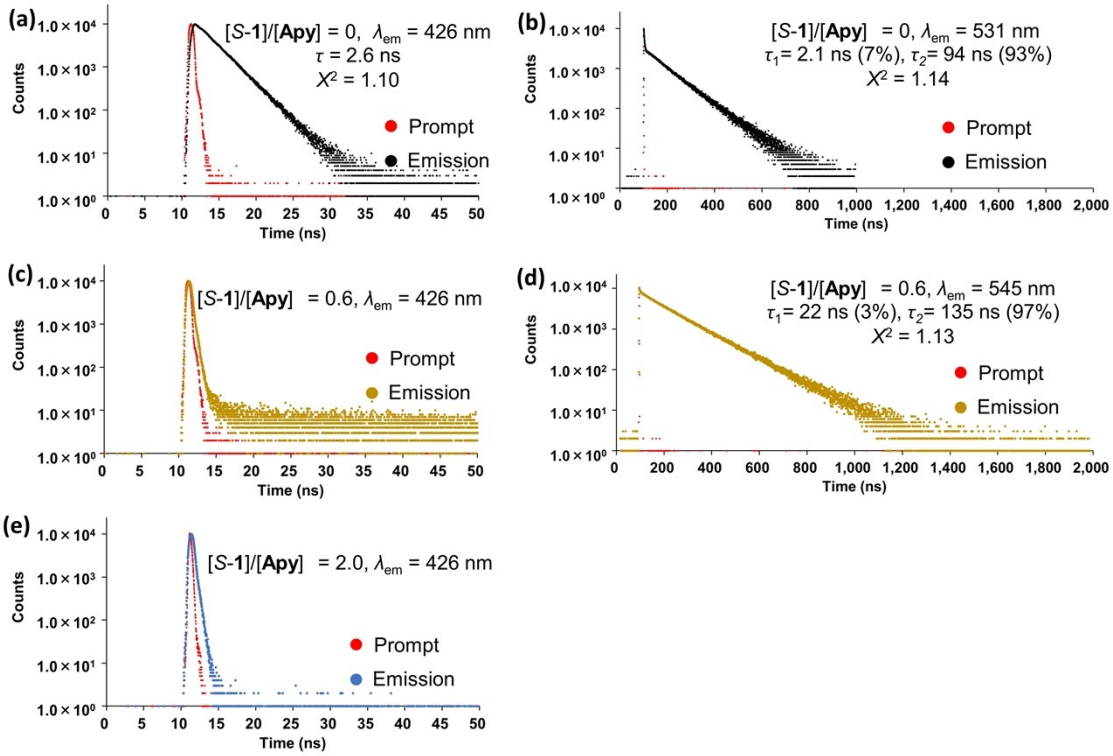

Fig. S34 Emission decays of **APy** (6 × 10^{-5} M) at various equiv. of *S*-**1**: (a, b) 0 equiv.; (c, d) 0.6 equiv.; (e) 2.0 equiv. The monitoring wavelength of (a, c, e) was 426 nm, that of (b) was 531 nm, and of (d) was 545 nm. All spectra were recorded at room temperature, λ_{ex} = 369 nm. The observations suggested that both monomers and excimers were present in the solution of **APy** (6 × 10^{-5} M), while further stacking occurred upon addition of 0.6 equiv. of *S*-**1**. In the sample of **APy** with 2.0 equiv. of *S*-**1**, where only the emission at ca. 426 nm was observed, the life time of monomer emission could not be measured due to the weak fluorescence intensity.

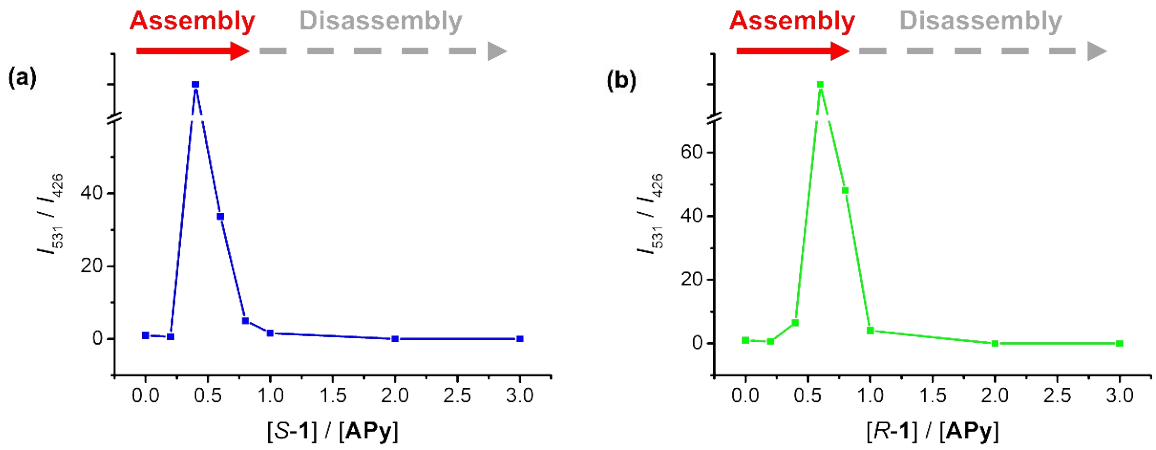

Fig. S35 Plots of the ratio between fluorescence intensities at 531 nm and 426 nm against the molar ratio between (a) *S*-**1** and **APy** and (b) *R*-**1** and **APy**.

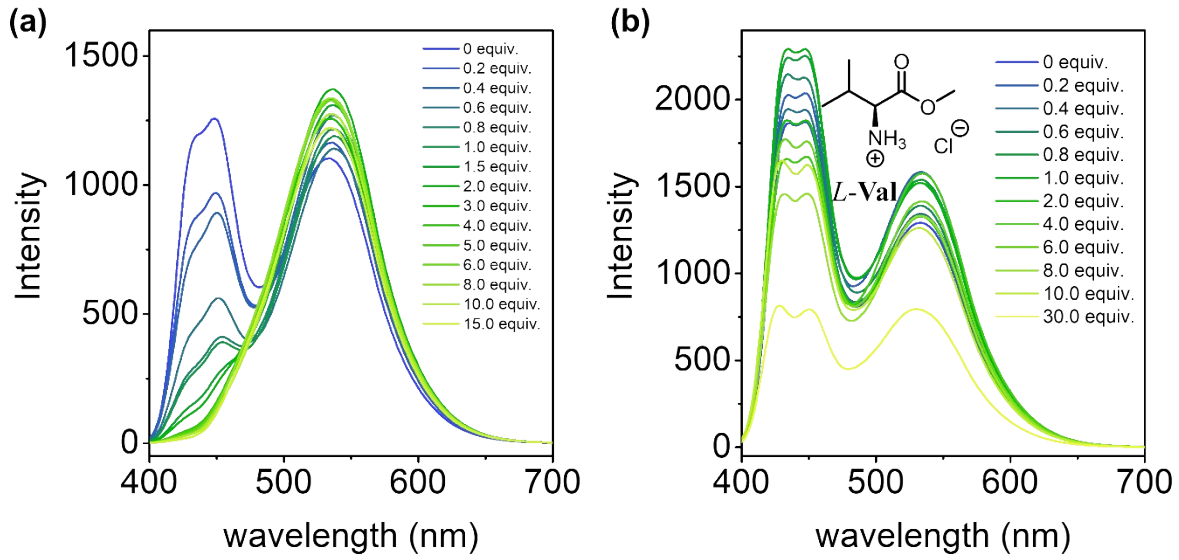

Fig. S36 Fluorescence spectra (λ_{ex} = 385 nm) of **APy** (6×10^{-5} M) upon addition of (a) *R*-**unit** and (b) *L*-**Val**. All spectra were recorded at room temperature. (a) Only the process of assembly was observed in case of titration with *R*-**unit**. (b) The fluorescent emission at *ca*. 426 nm did not disappear during the whole titration. The ratio of I_{426} and I_{530} slightly changed, indicating that *L*-**Val** triggered the assembly of **APy** with low efficiency.

CPL of APy upon addition of 1

Table S3. Quantum yields of **APy** upon addition of chiral **1**.[a]

	S-**1**	*R*-**1**
0 equiv.	67%	69%
0.2 equiv.	63%	67%
0.4 equiv.	48%	50%
0.6 equiv.	43%	47%
0.8 equiv.	23%	27%
1.0 equiv.	10%	10%
2.0 equiv.	5%	5%

[a] The concentration of **APy** was 6×10^{-5} M.

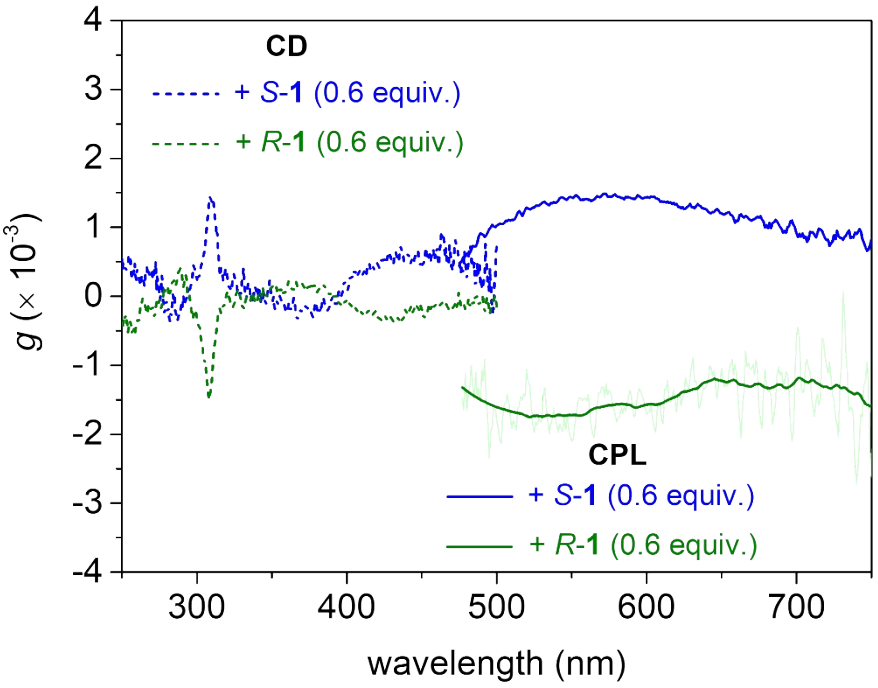

Fig. S37 The *g*-values of CD and CPL spectra of the aqueous solution of **APy** (6×10^{-5} M) with 0.6 equiv. of chiral **1**.

Supplementary discussion

The effect of **1** on the "assembly and disassembly" of **APy** was highly efficient. The concentration decrease of **APy** did not stop **1** from triggering assembly of **APy** (Fig. S38 and S39). Even at the concentration as low as 1×10^{-6} M, where the aqueous solution of **APy** was dominated by monomeric state, 0.4 equiv. of *S*-**1** accomplished the assembly of **APy**, while 2.0 equiv. of *S*-**1** caused complete disassembly of **APy**, as evidenced by the disappearance and appearance of fluorescence emission at *ca*. 426 nm (Fig. S39).

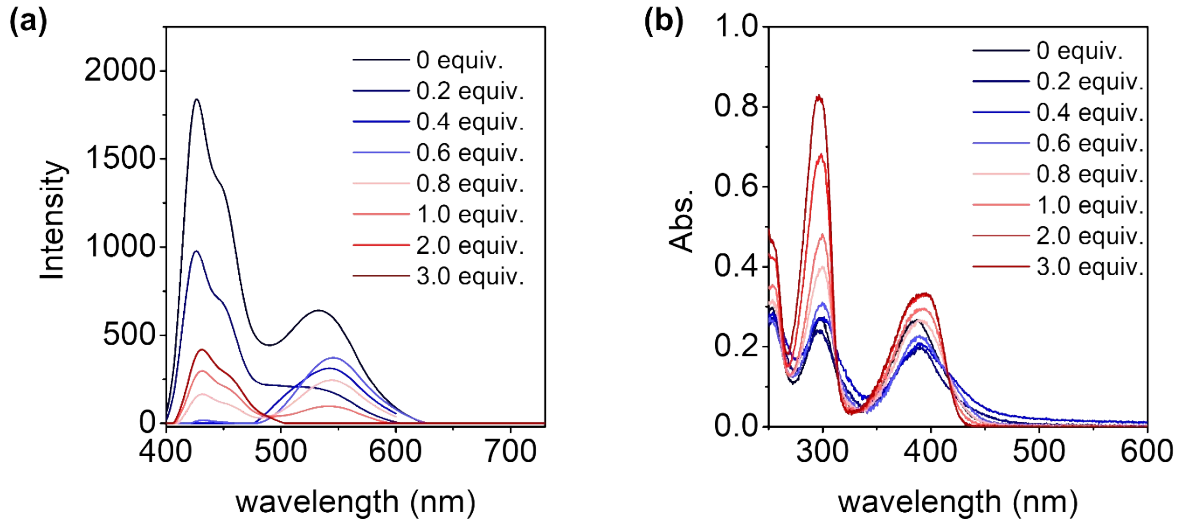

Fig. S38 (a) Fluorescence spectra (λ_{ex} = 385 nm) and (b) UV-vis spectra of **APy** (1×10^{-5} M) upon addition of *S*-**1**. All spectra were recorded at room temperature.

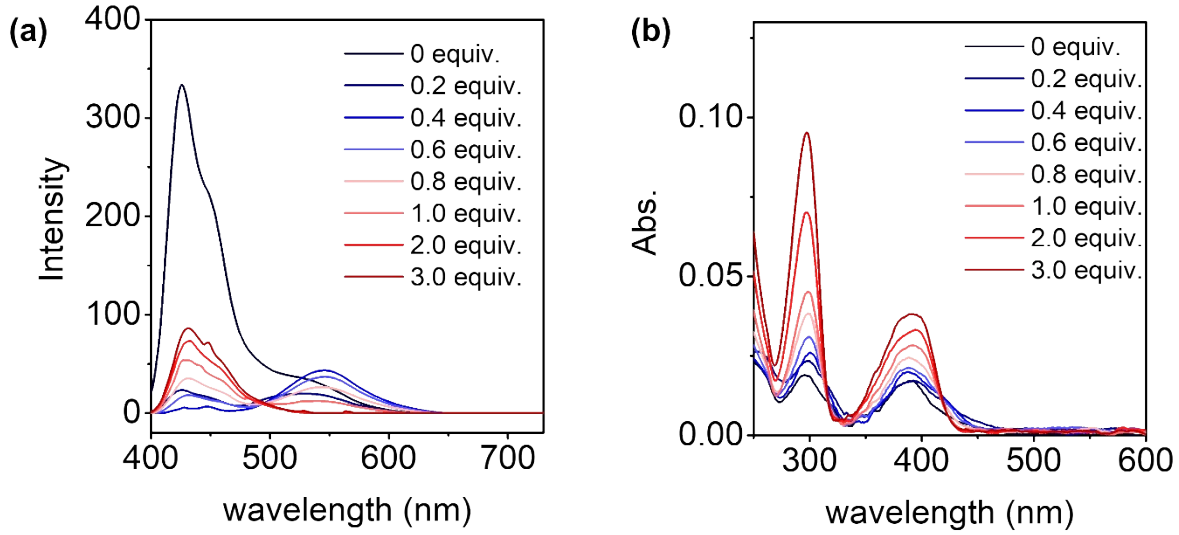

Fig. S39 (a) Fluorescence spectra (λ_{ex} = 385 nm) and (b) UV-vis spectra of **APy** (1×10^{-6} M) upon addition of *S*-**1**. All spectra were recorded at room temperature.

The host-guest complexation between **APy** and **1** and the planar chirality of **1** ensured the successful chiral transfer from chiral **1** to the assembly of **APy**. When a competitive guest, **C8**,

was added to the mixture of **Apy** and *R*-**1** in a 1 : 0.6 molar ratio, the CD signal of **APy** gradually disappeared as the competitive complexation between *R*-**1** and **C8** (Fig. S40).

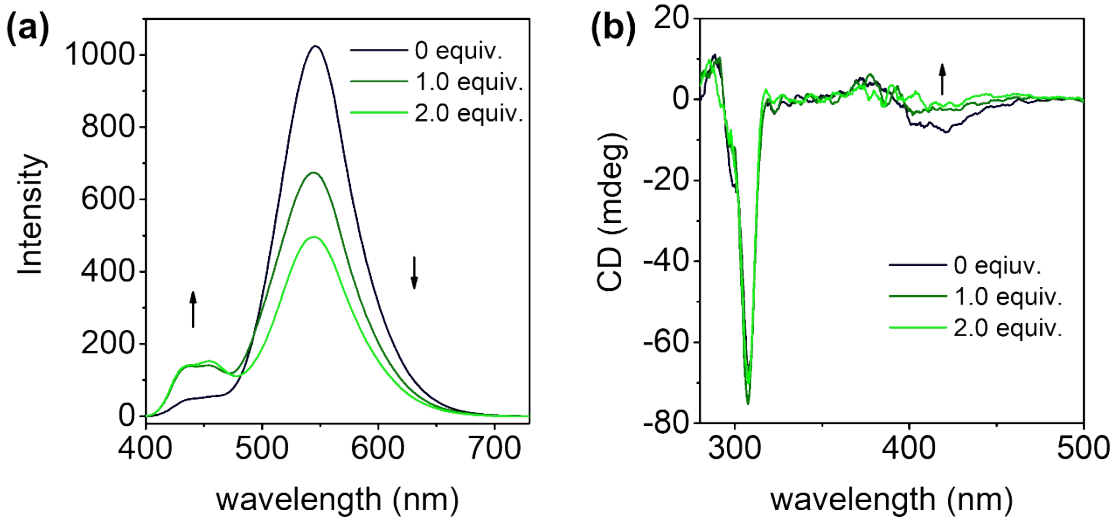

Fig. S40 (a) Fluorescence and (b) CD spectra of the mixture of **APy** (6×10^{-5} M) and *R*-**1** (3.6×10^{-5} M, 0.6 equiv.) upon addition of **C8**. Disassembly and loss of chirality of **APy** were observed.

References

S1 S. Fa, M. Mizobata, S. Nagano, K. Suetsugu, T. Kakuta, T.-A. Yamagishi and T. Ogoshi, *ACS Nano*, 2021, **15**, 16794–16801.

S2 Y. Xu, D. Chang, S. Feng, C. Zhang and J.-X. Jiang, *New J. Chem.*, 2016, **40**, 9415–9423.

S3 G. Colombano, C. Travelli, U. Galli, A. Caldarelli, M. G. Chini, P. L. Canonico, G. Sorba, G. Bifulco, G. C. Tron and A. A. Genazzani, *J. Med. Chem.*, 2010, **53**, 616–623.

S4 T. Ogoshi, S. Kanai, S. Fujinami, T. Yamagishi and Y. Nakamoto, *J. Am. Chem. Soc.*, 2008, **130**, 5022−5023.

S5 J. Park, Y. Choi, S. S. Lee and J. H. Jung, *Org. Lett.*, 2019, **21**, 1232−1236.

S6 N. L. Strutt, H. Zhang and J. F. Stoddart, *Chem. Commun*., 2014, **50**, 7455−7458.

S7 T. Ogoshi, K. Masaki, R. Shiga, K. Kitajima and T. Yamagishi, *Org. Lett.*, 2011, **13**, 1264−1266.

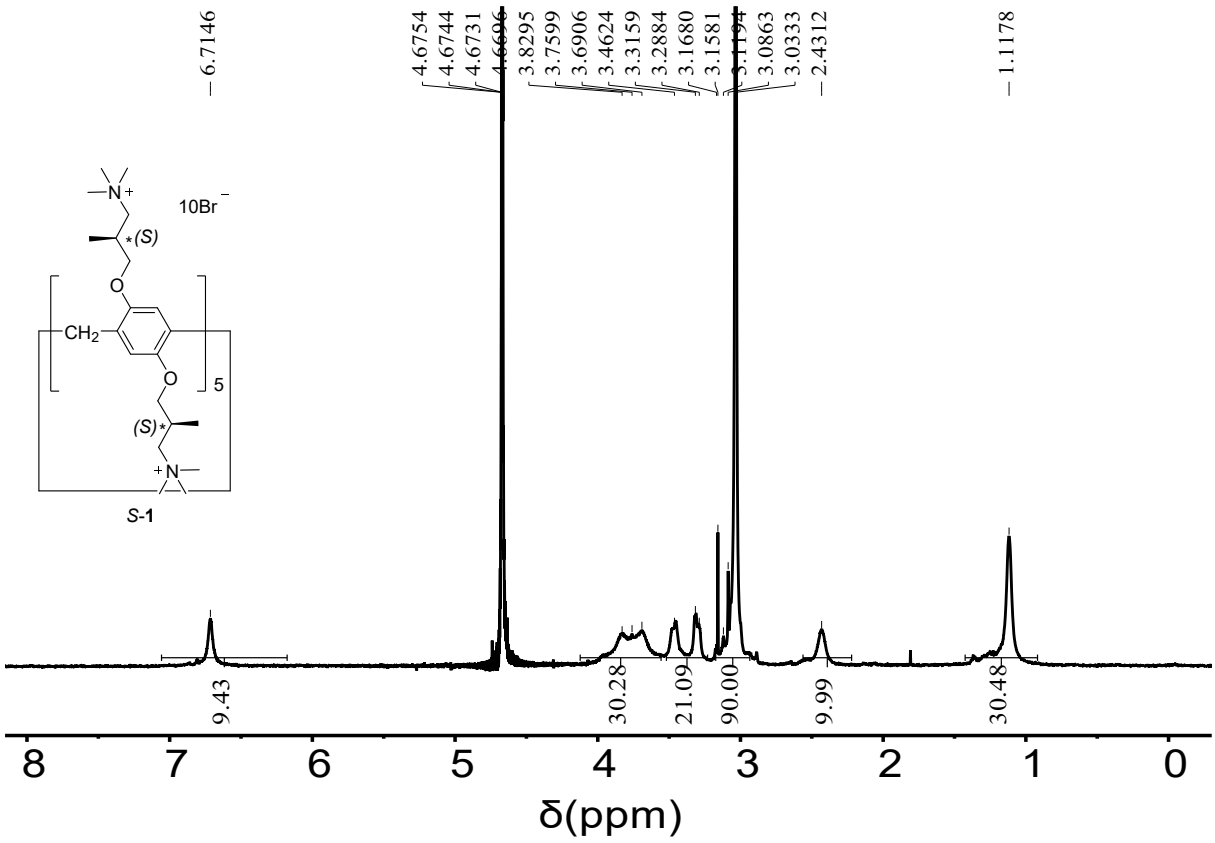
6.7146
4.6754
4.6744
4.6731
4.6696
3.8295
3.7599
3.6906
3.4624
3.3159
3.2884
3.1680
3.1581
3.1194
3.0863
3.0333
2.4312
1.1178
10Br⁻
*(S)
O
CH2
O
5
(S)*
+N
S-1
9.43
30.28
21.09
90.00
9.99
30.48
8
7
6
5
4
3
2
1
0
δ(ppm)

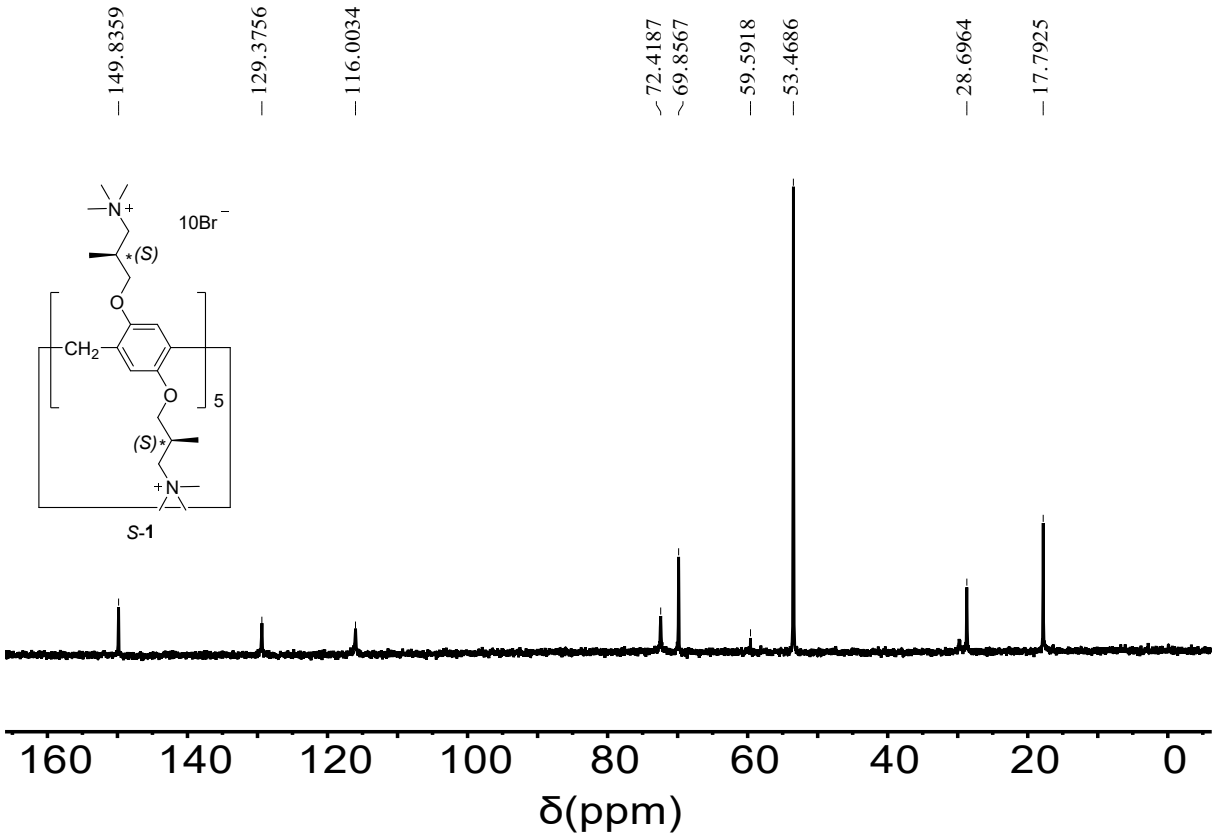
149.8359
129.3756
116.0034
72.4187
69.8567
59.5918
53.4686
28.6964
17.7925
10Br⁻
*(S)
O
CH2
O
5
(S)*
+N
S-1
160
140
120
100
80
60
40
20
0
δ(ppm)

^{1}H & ^{13}C NMR Spectra (D_2O, 25 °C)

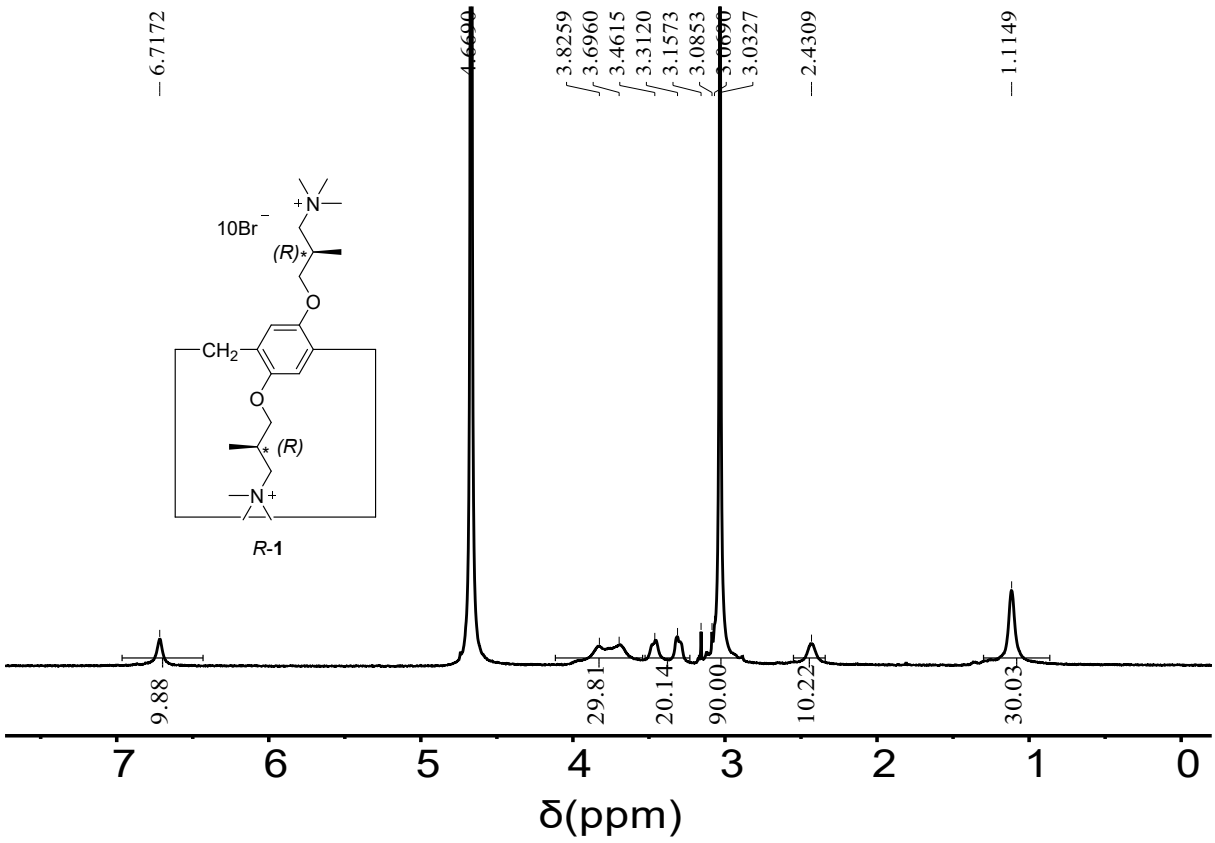

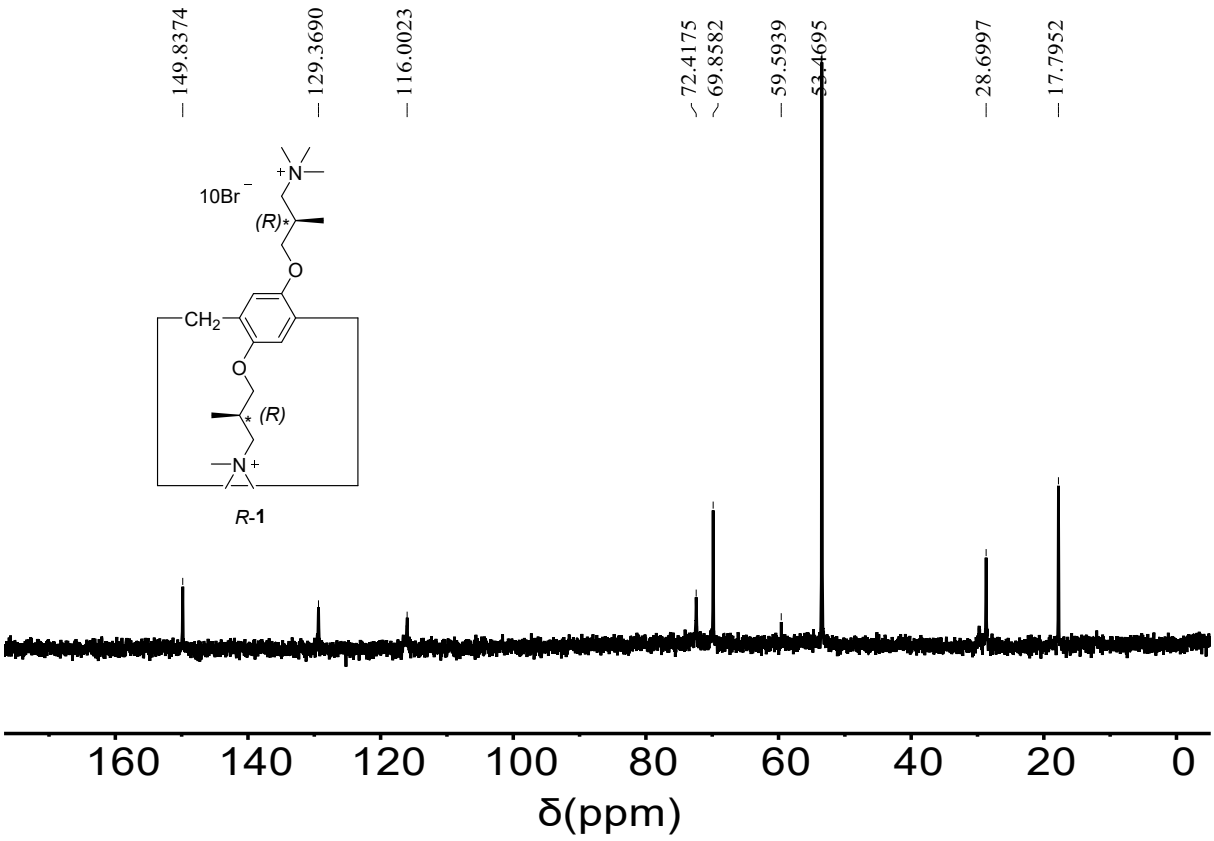

^{1}H & ^{13}C NMR Spectra (D_2O, 25 °C)

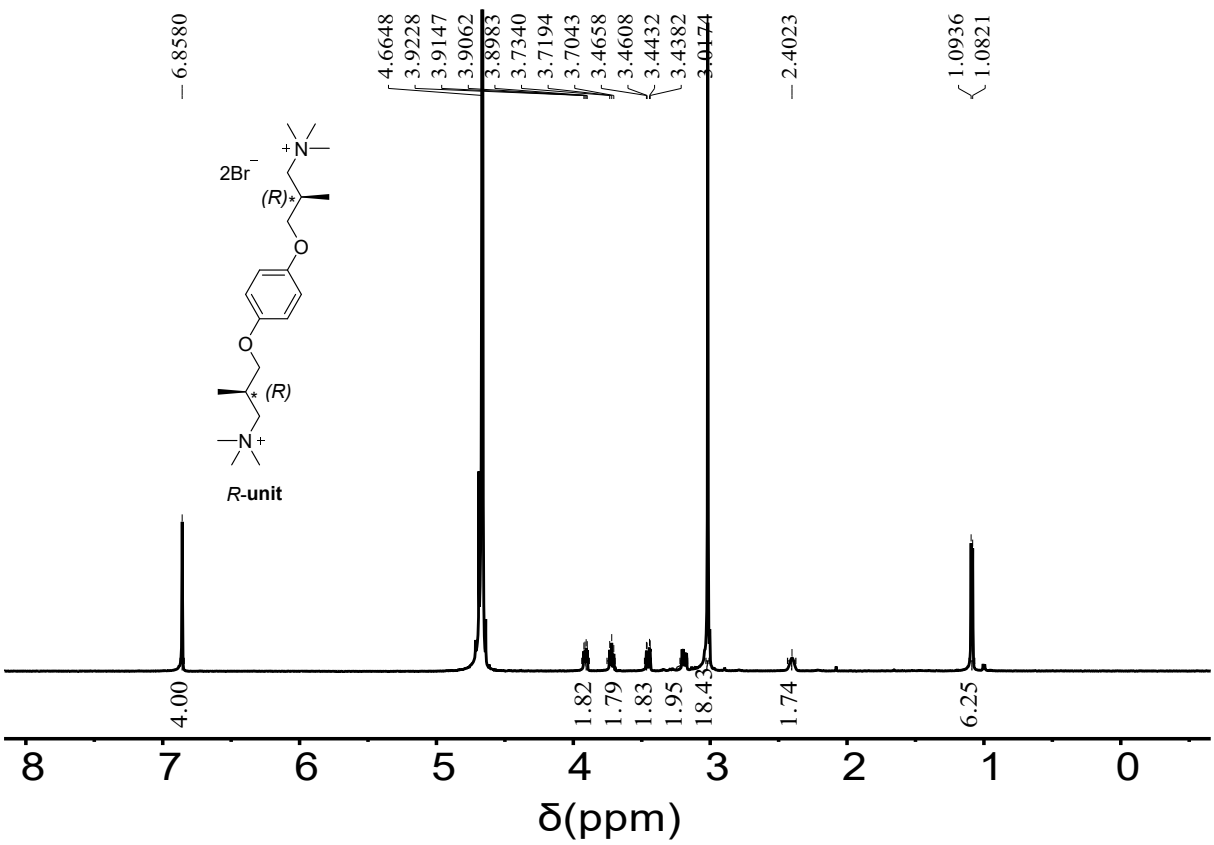

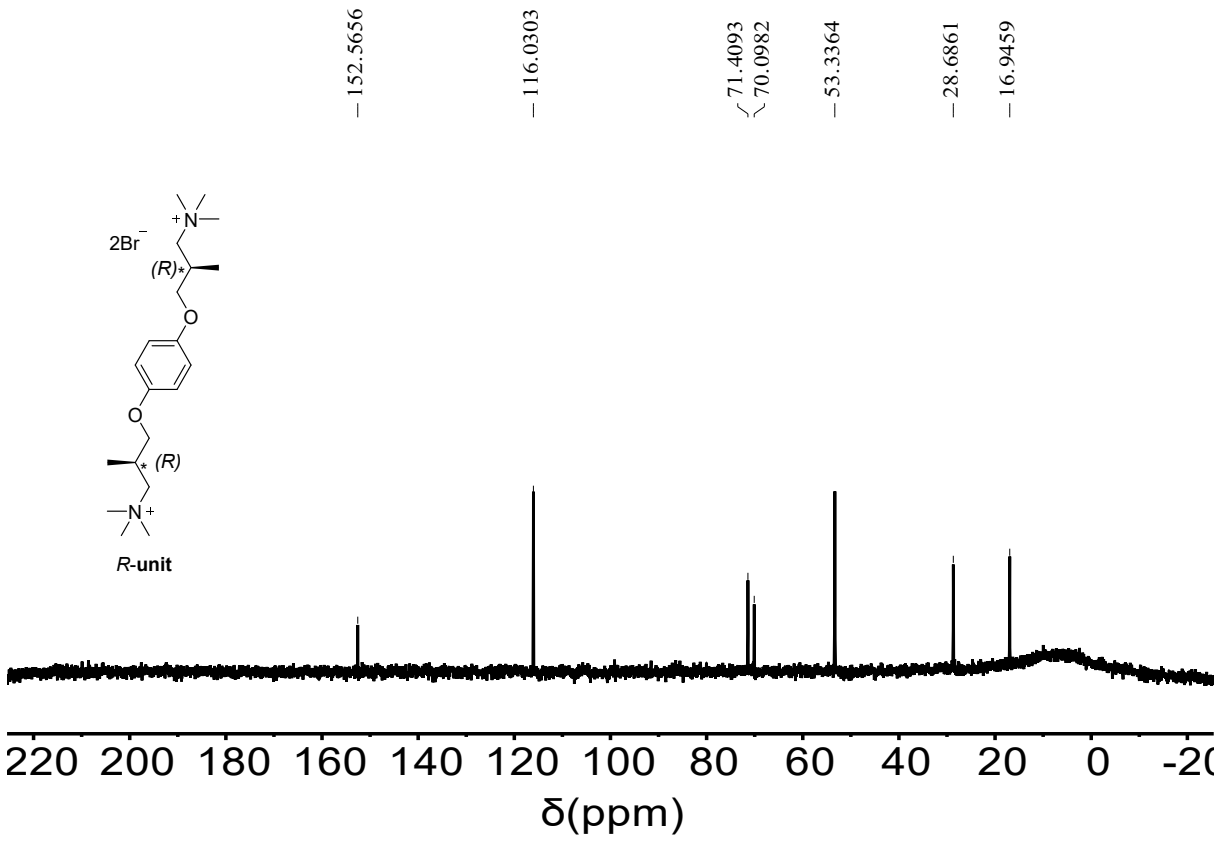

^{1}H & ^{13}C NMR Spectra (D_2O, 25 °C)

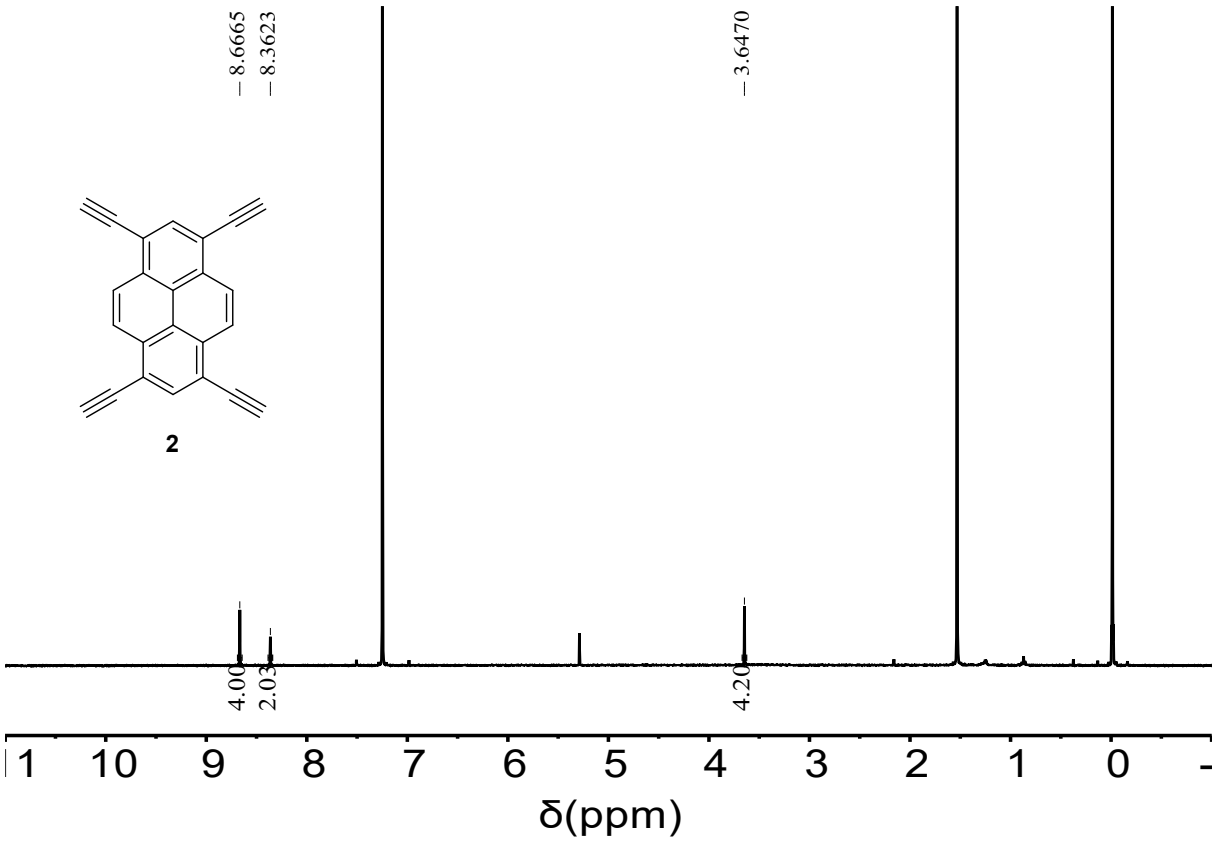
8.6665
8.3623
3.6470
2
4.00
2.03
4.20
δ(ppm)

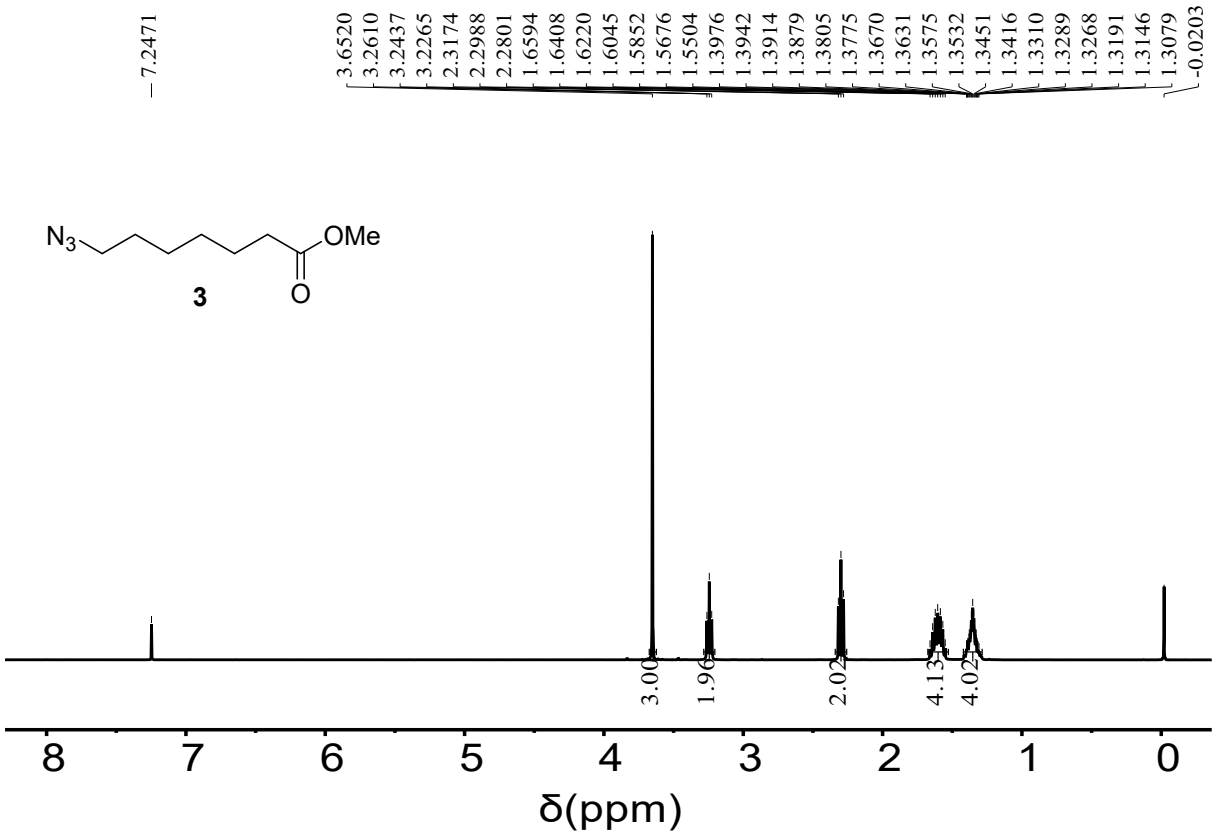
7.2471
3.6520
3.2610
3.2437
3.2265
2.3174
2.2988
2.2801
1.6594
1.6408
1.6220
1.6045
1.5852
1.5676
1.5504
1.3976
1.3942
1.3914
1.3879
1.3805
1.3775
1.3670
1.3631
1.3575
1.3532
1.3451
1.3416
1.3310
1.3289
1.3268
1.3191
1.3146
1.3079
-0.0203
N3
OMe
O
3
3.00
1.96
2.02
4.13
4.02
δ(ppm)

^{1}H NMR Spectra of **2** and **3** ($CDCl_3$, 25 °C)

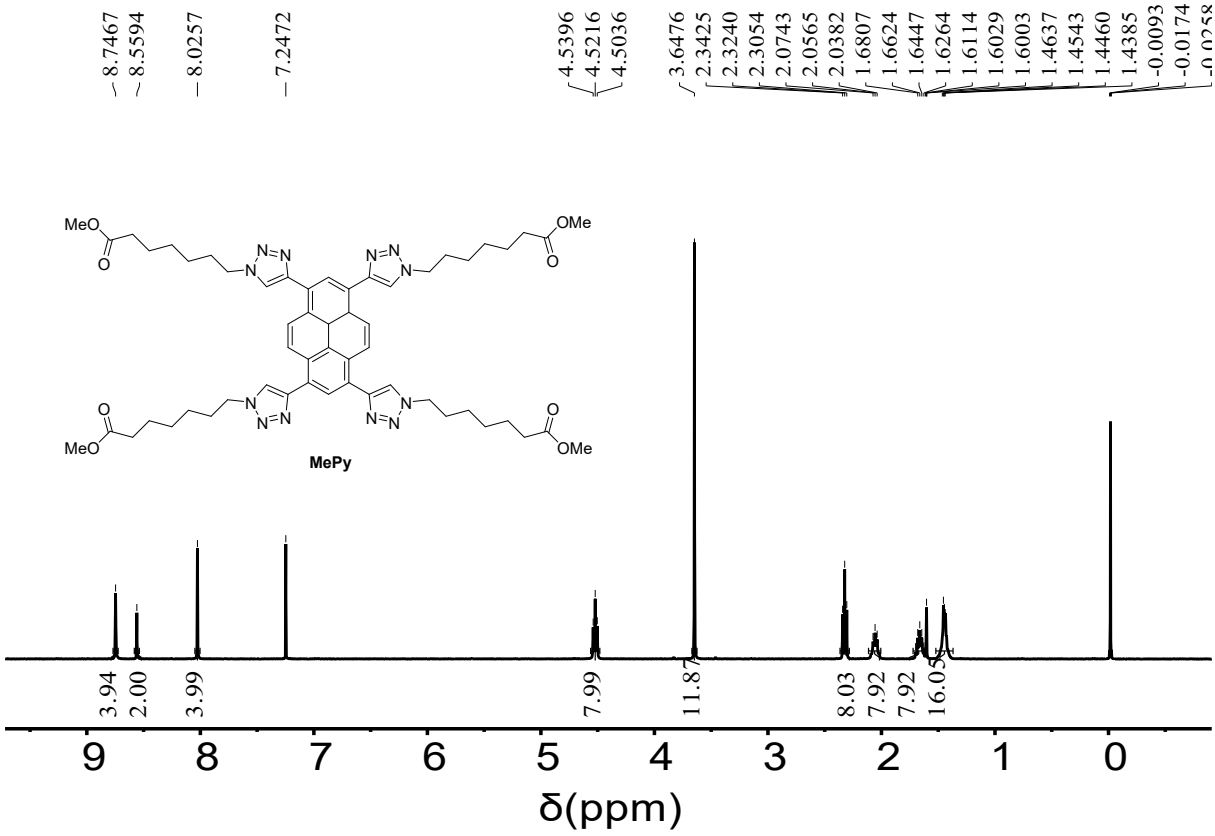

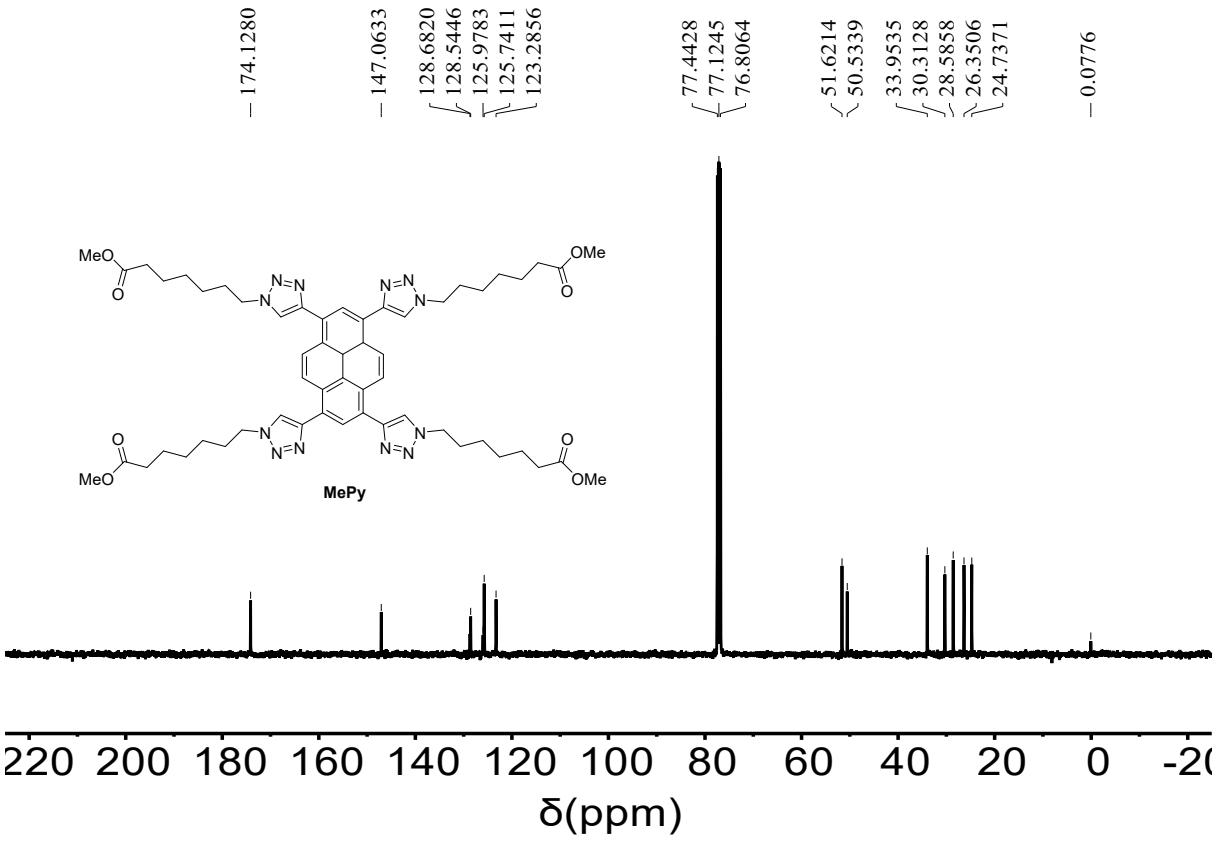

^{1}H & ^{13}C NMR Spectra ($CDCl_3$, 25 °C)

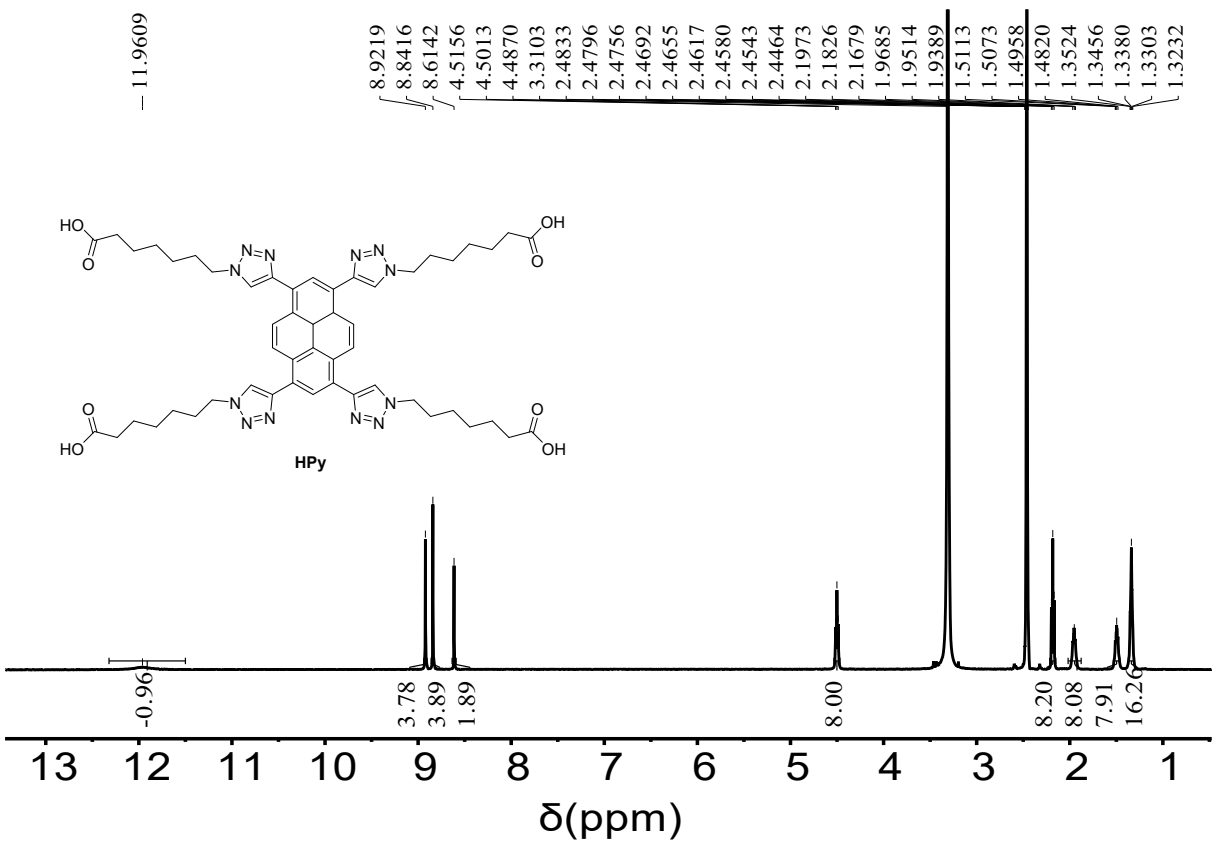

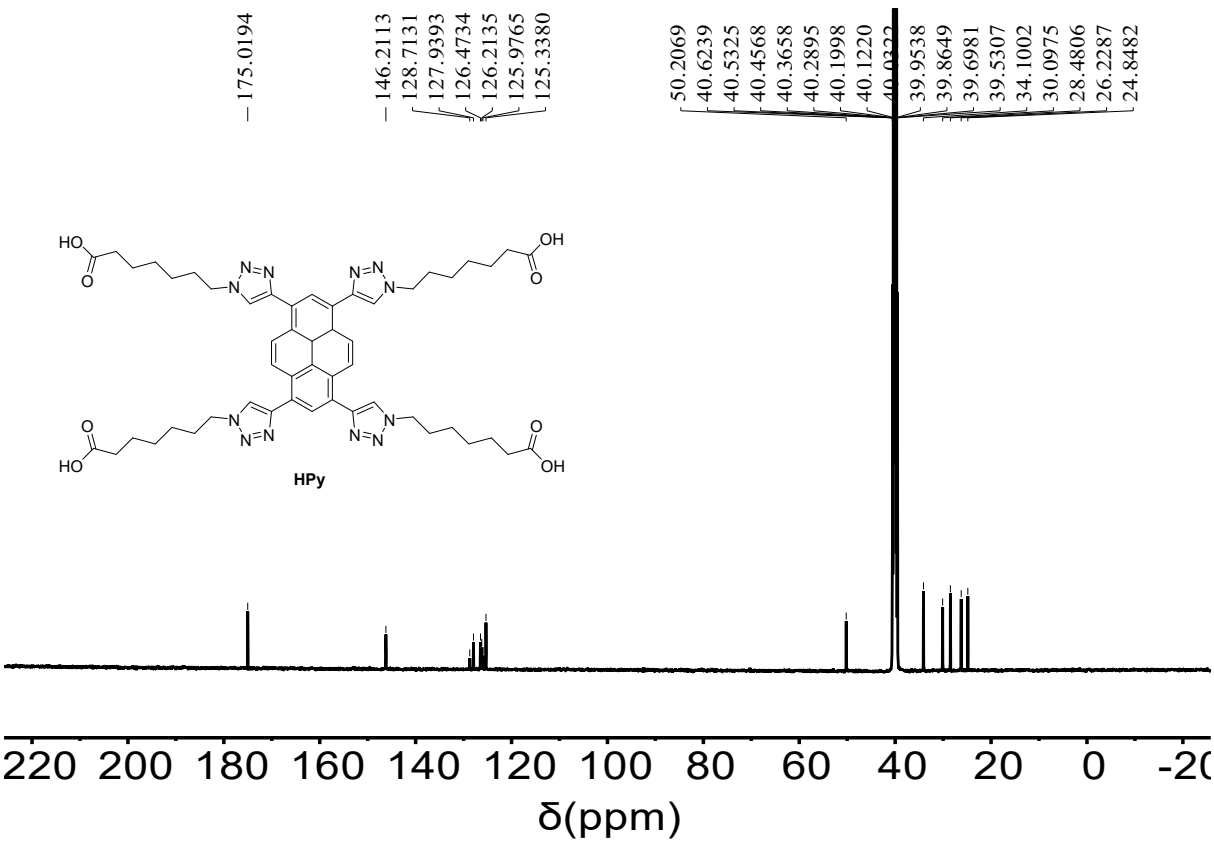

^{1}H & ^{13}C NMR Spectra (DMSO-d_6, 25 ^{o}C)

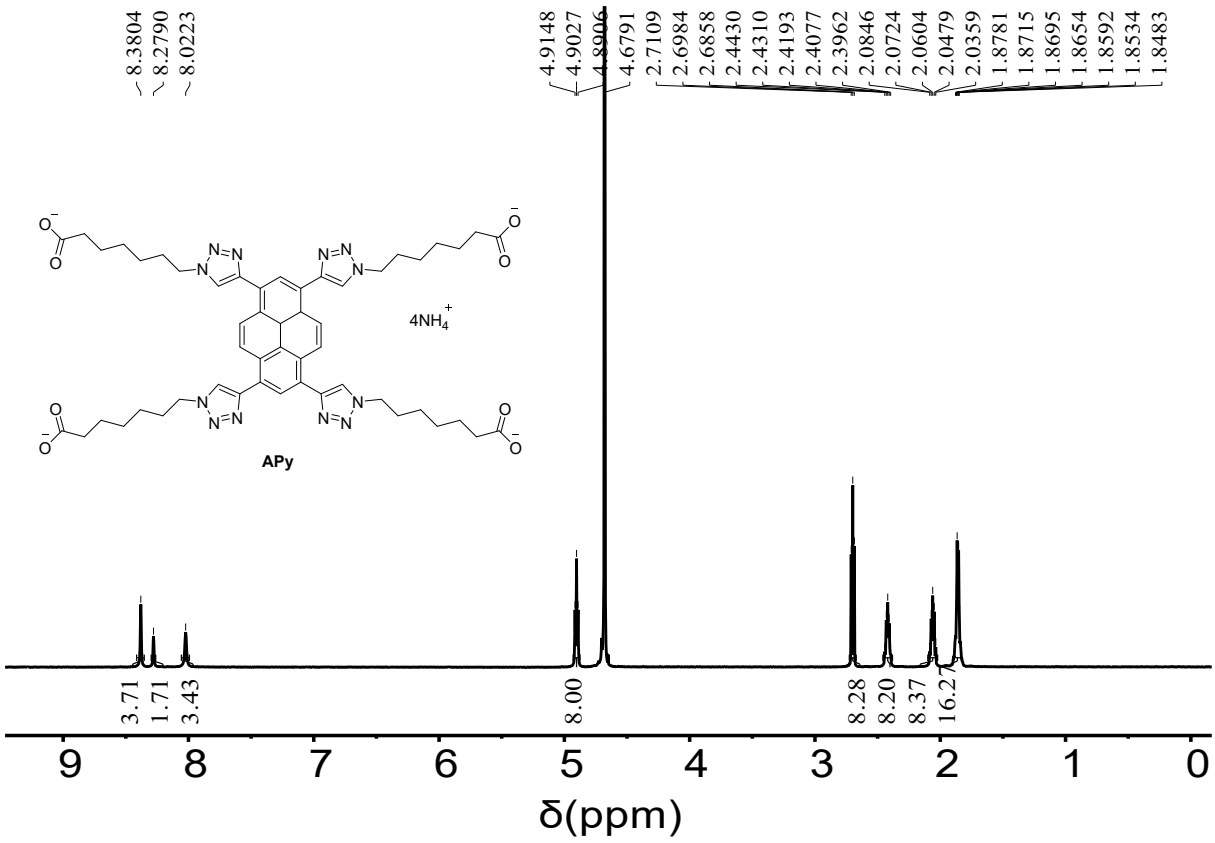
8.3804
8.2790
8.0223
4.9148
4.9027
4.8906
4.6791
2.7109
2.6984
2.6858
2.4430
2.4310
2.4193
2.4077
2.3962
2.0846
2.0724
2.0604
2.0479
2.0359
1.8781
1.8715
1.8695
1.8654
1.8592
1.8534
1.8483
4NH4+
APy
3.71
1.71
3.43
8.00
8.28
8.20
8.37
16.27
9
8
7
6
5
4
3
2
1
0
δ(ppm)

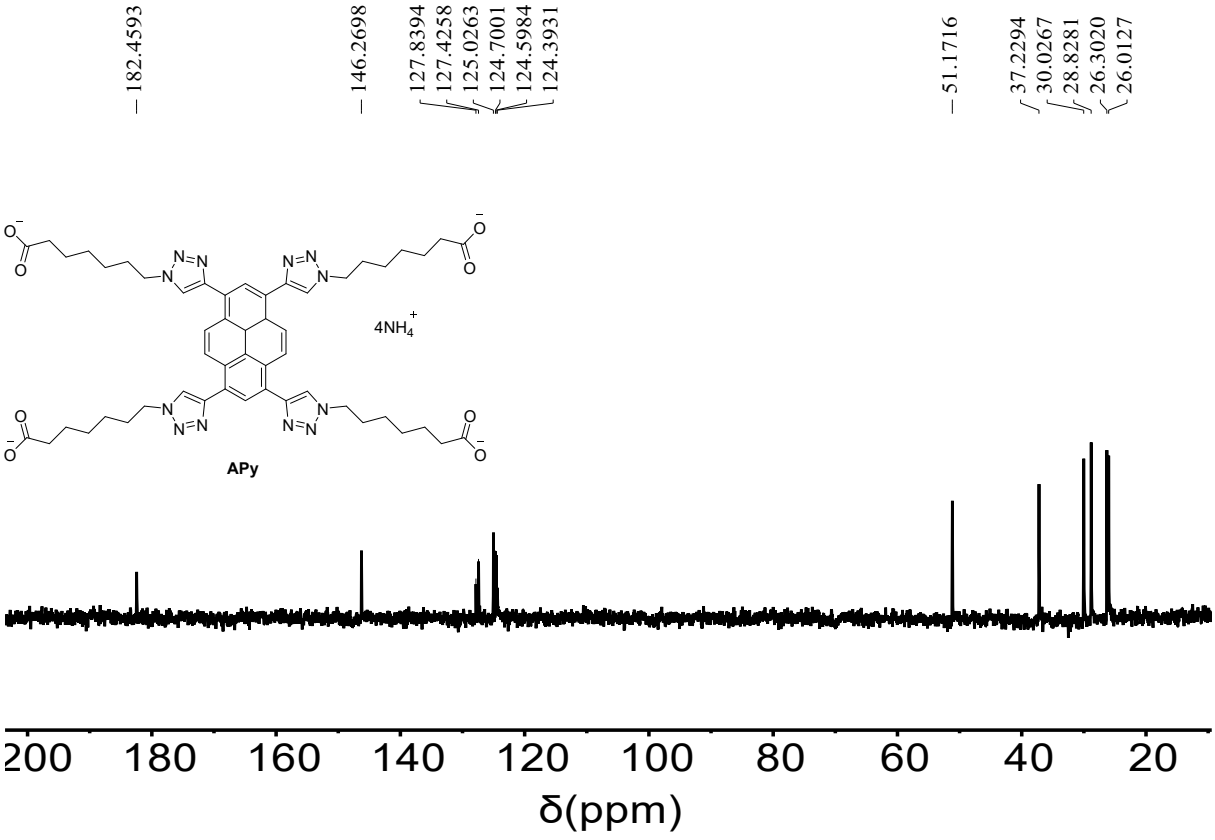
182.4593
146.2698
127.8394
127.4258
125.0263
124.7001
124.5984
124.3931
51.1716
37.2294
30.0267
28.8281
26.3020
26.0127
4NH4+
APy
200
180
160
140
120
100
80
60
40
20
δ(ppm)

^{1}H & ^{13}C NMR Spectra (D_2O, 25 °C)

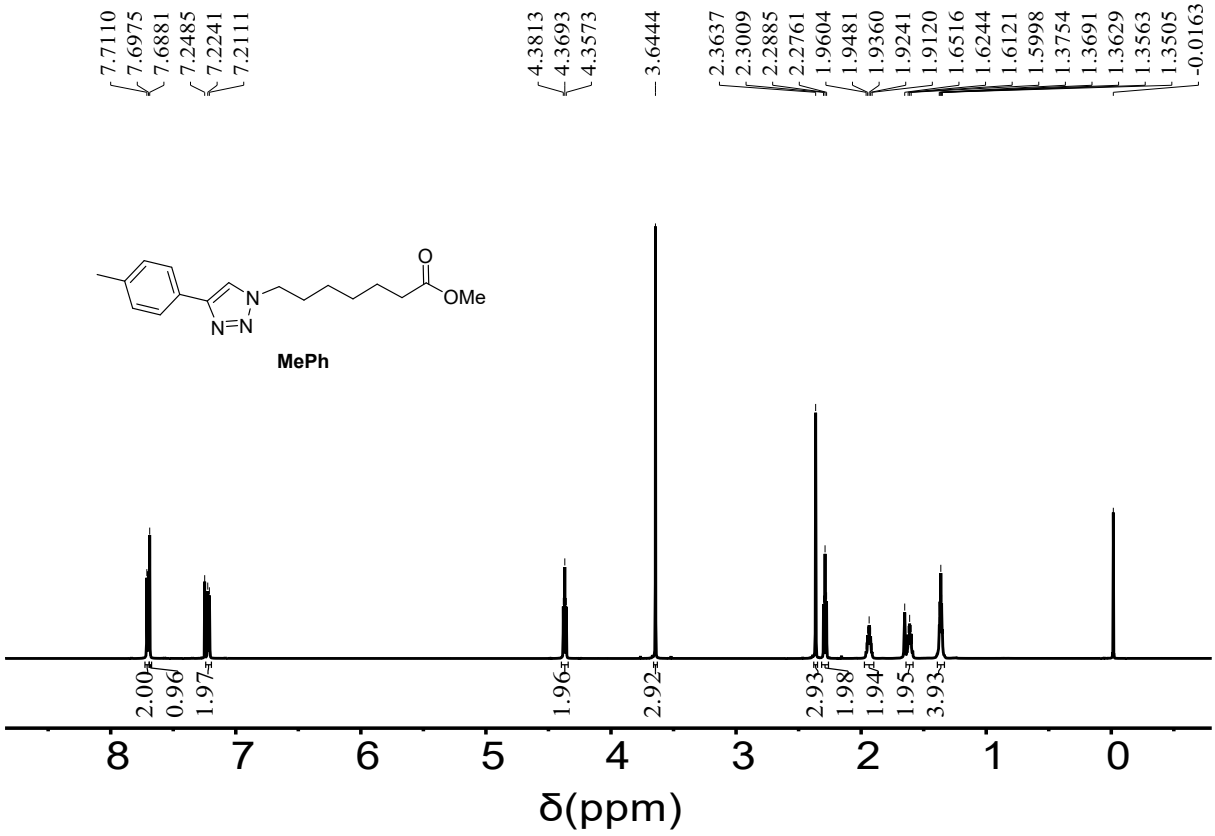

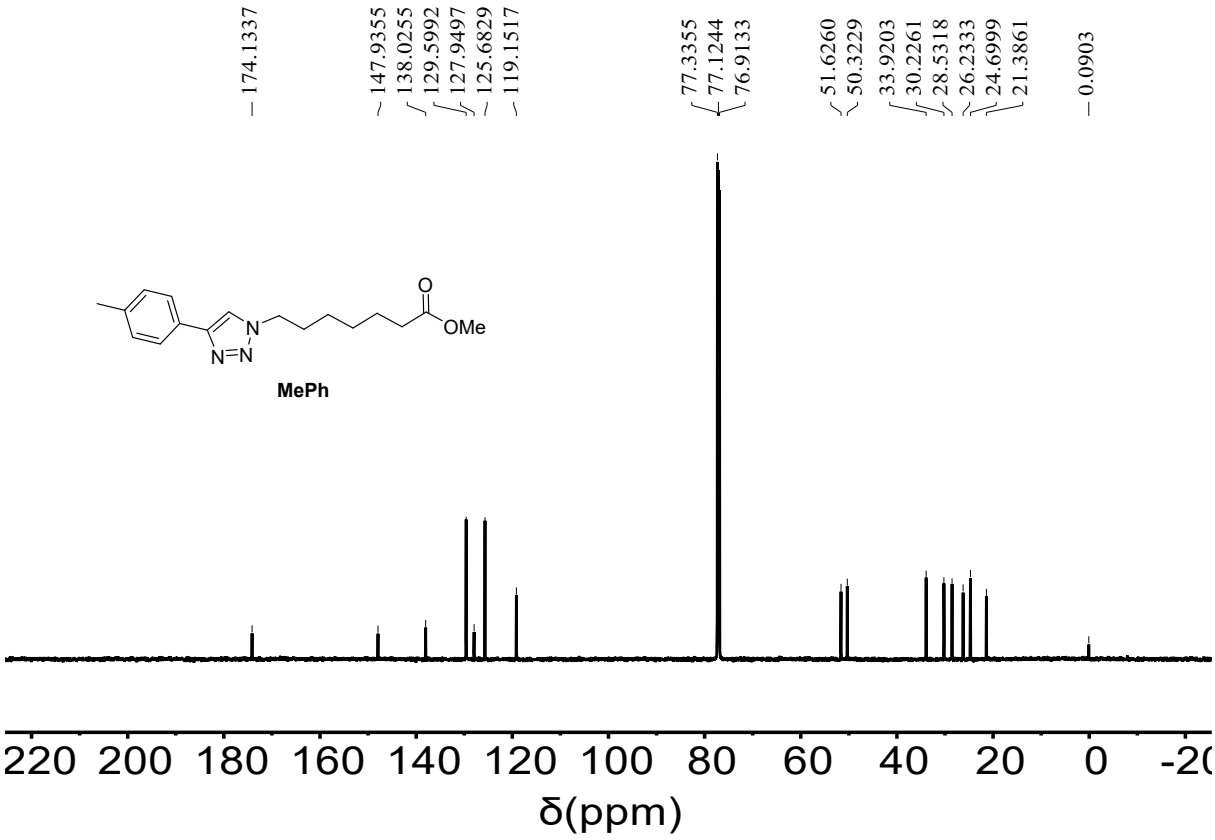

^{1}H & ^{13}C NMR Spectra ($CDCl_3$, 25 °C)

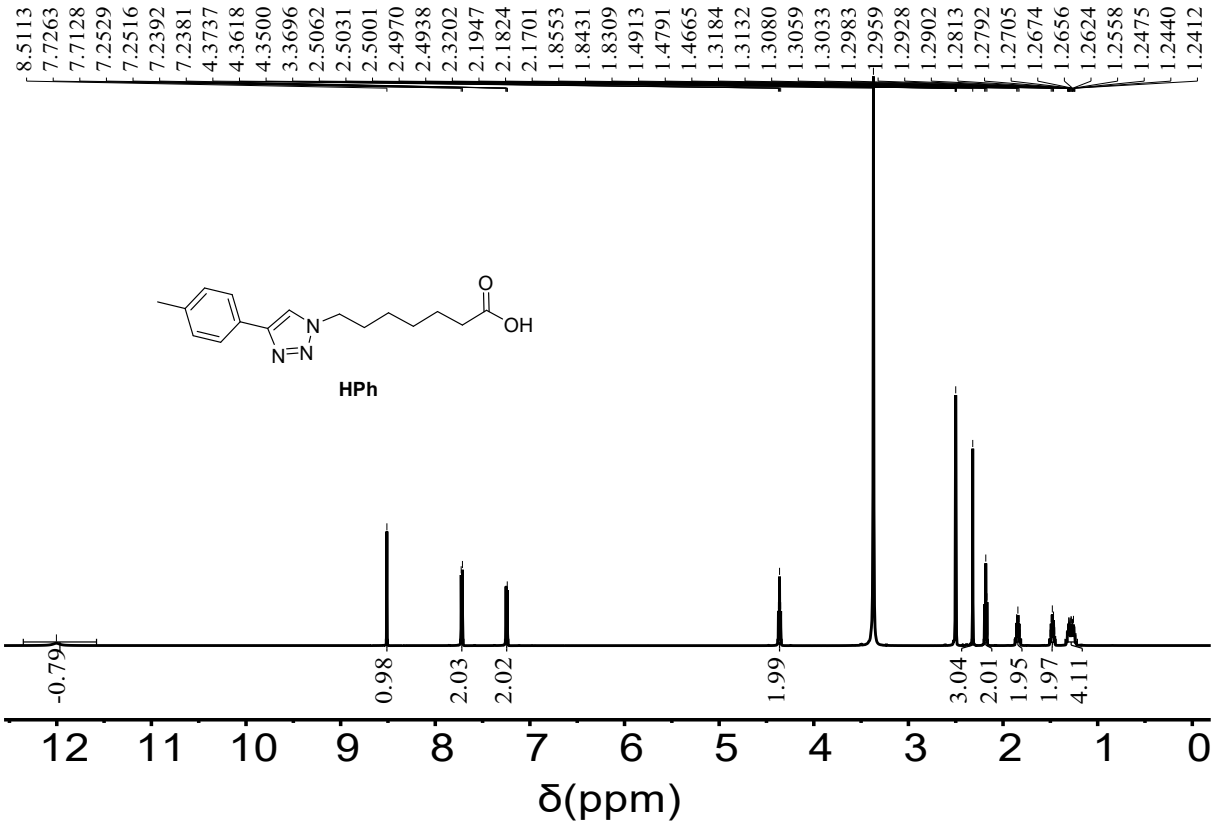

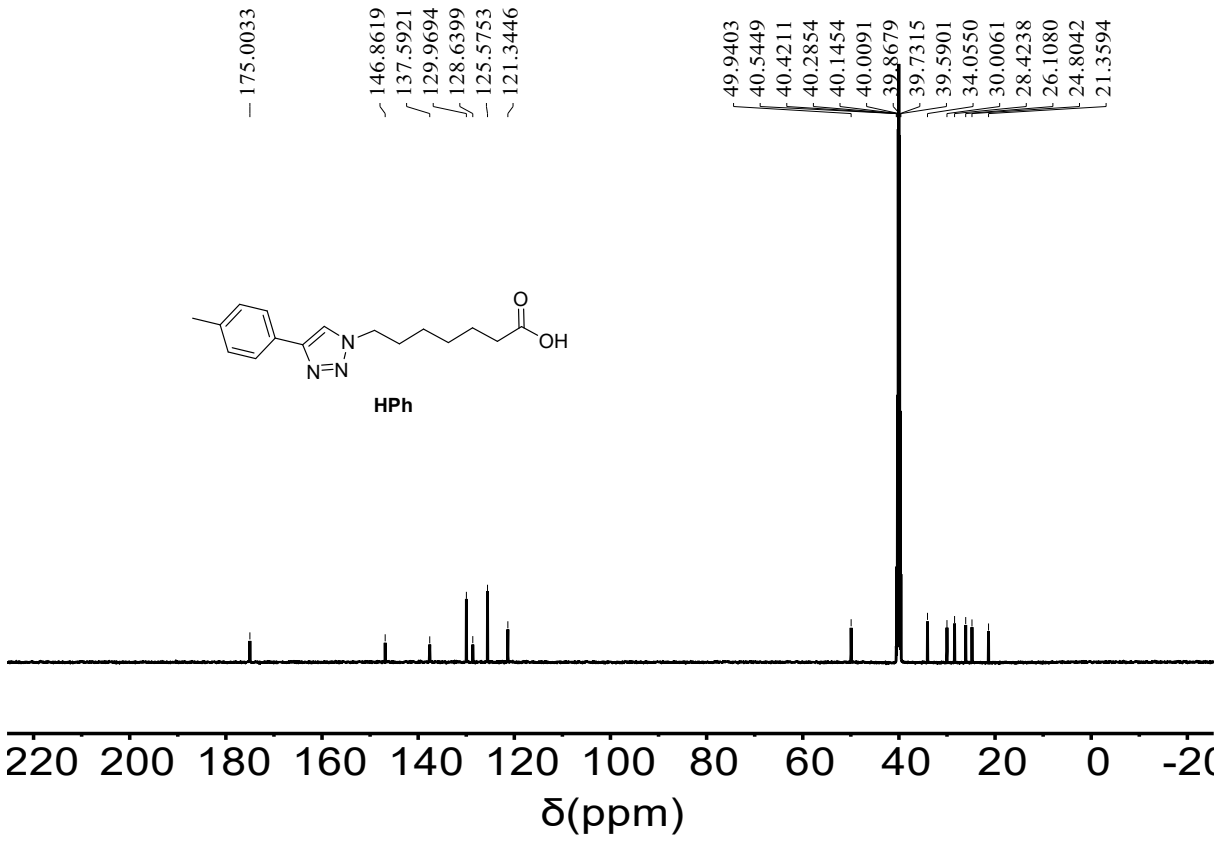

^{1}H & ^{13}C NMR Spectra (DMSO-d_6, 25 ^{o}C)

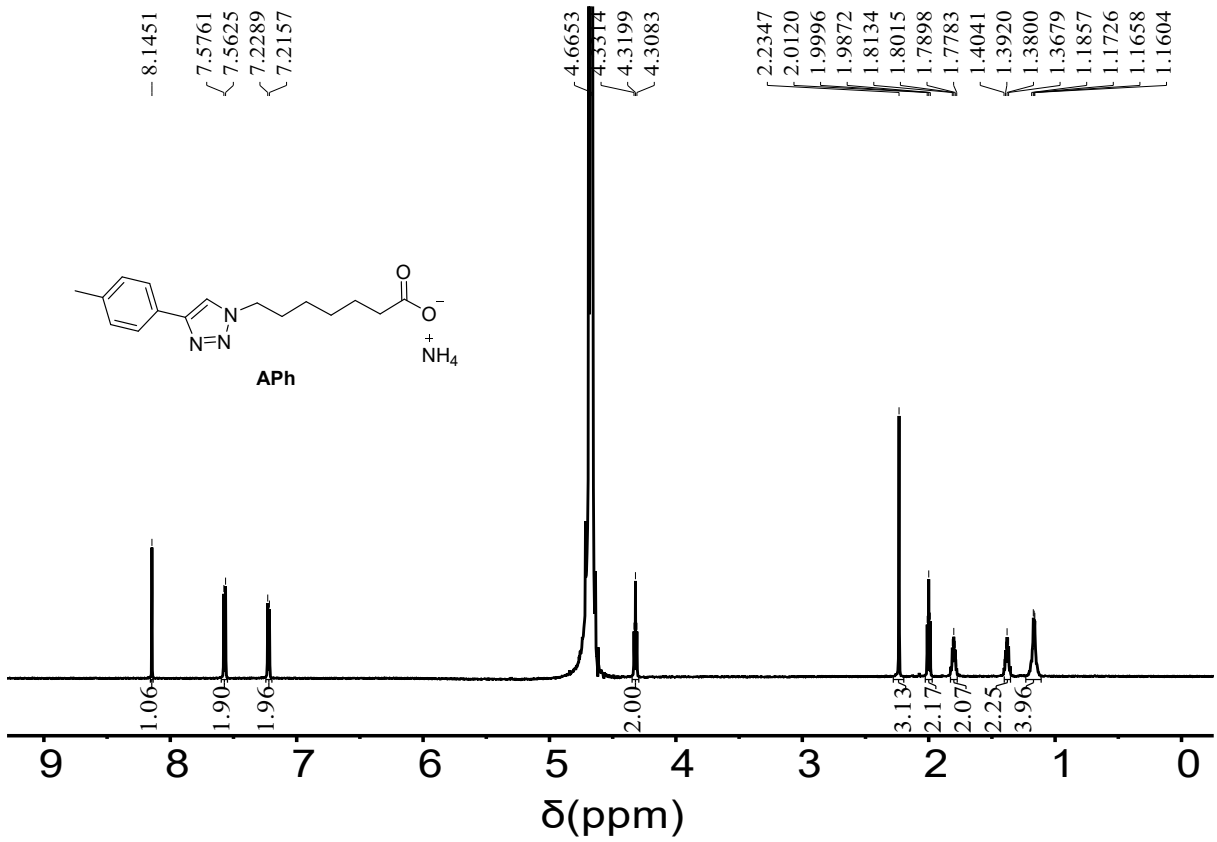

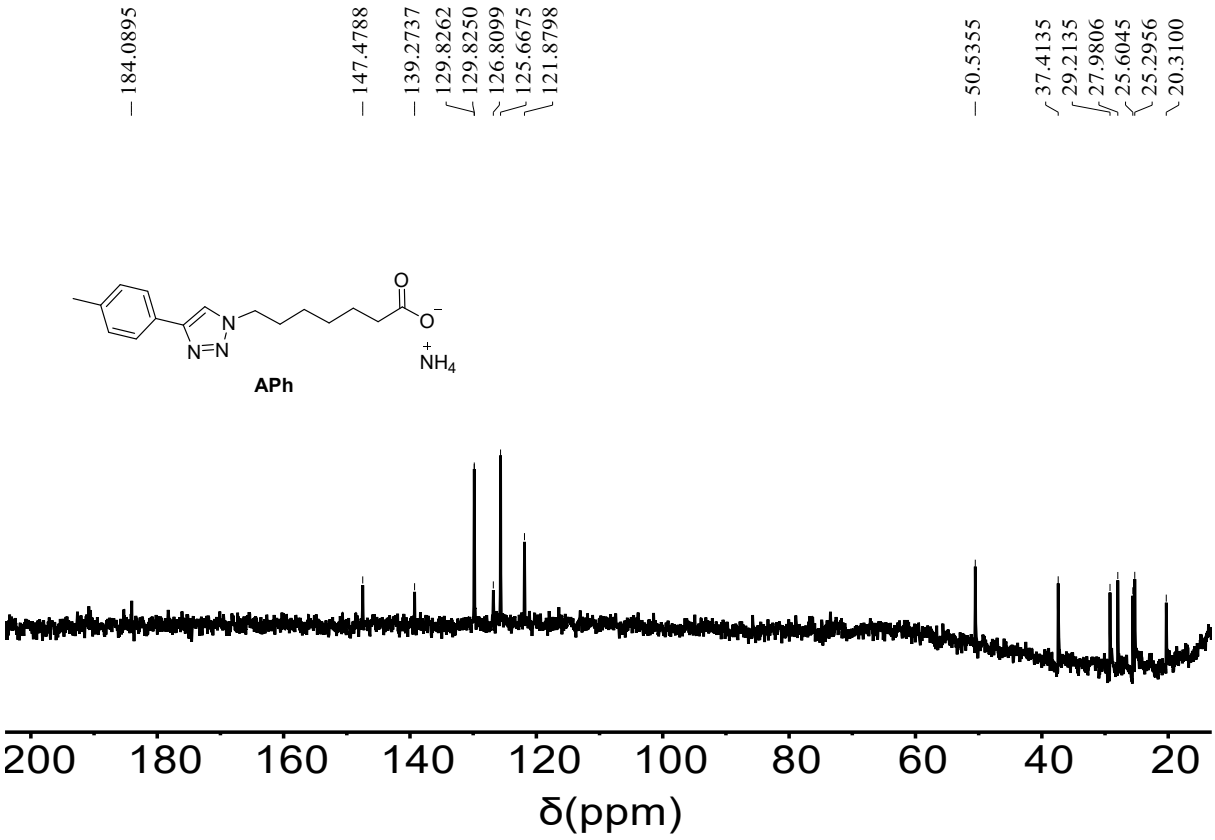

^{1}H & ^{13}C NMR Spectra (D_2O, 25 ^{o}C)